Journal of Hydrology: Regional Studies 50 (2023) 101580

Contents lists available at ScienceDirect

Journal of Hydrology: Regional Studies

journal homepage: www.elsevier.com/locate/ejrh

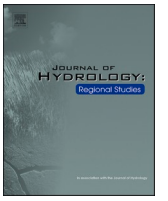

Deriving synthetic rating curves from a digital elevation model to delineate the inundated areas of small watersheds

Camila A. Gordon *, Etienne Foulon, Alain N. Rousseau

Institut national de la recherche scientifique (INRS), Centre Eau Terre Environnement, 490 rue de la Couronne, Québec, QC G1K 9A9, Canada

ARTICLE INFO

Keywords:
Floodplain mapping
Height above the nearest drainage
Global sensitivity analysis
Manning equation

ABSTRACT

Study region: Two southern Quebec (Canada) watersheds were used to validate the proposed method for delineating inundated areas of small watersheds: the 554-km2 St.Charles and the 133 km2 À la Raquette watersheds. Observed data from six-gauge stations were used to validate the Synthetic Rating Curves (SRC) developed in the study.
Study focus: This research focuses on the application of the Height Above the Nearest Drainage (HAND) method to derive SRCs and support floodplain mapping in small watersheds.
Accurate floodplain delineation is crucial of flood management, particularly in datascarce regions. This study presents a novel approach using (HAND) approach to precisely identify flood-prone areas. It involves generating (SRCs) connecting discharge and terrain derived hydraulic characteristics, integrated into PHYSITEL; a Geographic Information System (GIS) for distributed hydrological modeling. The Froude number established a consistent relationship between mean discharge and water depth across various discharge levels, defining unique hydraulic regimes. A Global Sensitivity Analysis quantified the uncertainty associated with SRC parameters, guiding calibration efforts to achieve biases below 20%. For both watersheds, postcalibration results showed SRCs with NRMSE values between 0.03 and 0.62. HANDSRC-based inundated areas corroborated the Quebec City flood risk zones well, with over 70% recall and 90% precision, validating its efficacy. These results contribute significantly to the region by providing SRCs for ungauged river sections and delineating first-hand floodplain maps.

1. Introduction

Globally, floods represent the most economically damaging natural disaster, accounting for 31% of losses (Yahaya, 2008). In Canada, flooding is the costliest natural disaster, with annual insurance claims exceeding one billion dollars (IBC, 2020). Beyond financial impacts, floods result in fatalities, population displacements, and structural damages every year (Hirabayashi et al., 2013; Jonkman, 2005). Severe flooding in Quebec and Ontario in 2017 and 2019 exceeded 100-year flood levels (ECCC, 2020; Zokagoa et al., 2021). The 2019 flooding in Ontario impacted over 310 municipalities and forced the evacuation of approximately 12,000 residents (Turcotte et al., 2019; Zokagoa et al., 2021). Given the influence of climate change on floods, accurate flood risk maps and effective mitigation strategies become essential tools for governments, municipalities, and flood risk managers.

Synthetic Rating Curves (SRC) relate discharge measurements or forecasts and water depths. These curves, referred as “synthetic” because they are derived from terrain-based data, offer an alternative to traditional floodplain mapping techniques. When combined

* Corresponding author.
E-mail address: Camila.gordon@inrs.ca (C.A. Gordon).

https://doi.org/10.1016/j.ejrh.2023.101580
Received 11 July 2023; Received in revised form 11 November 2023; Accepted 15 November 2023
Available online 27 November 2023

with low-complexity models, such as Height Above the Nearest Drainage (HAND), which leverages Digital Elevation Models (DEM) and the Manning equation they can be used to estimate the average hydraulic geometry and discharge of river reaches (Zheng et al., 2018). The HAND framework generates SRCs to delineate flood inundation areas. Although dependent on observations for calibration, this conceptual method meets the demand for efficient, reliable, and fast flood risk mapping tools (McGrath et al., 2018).

Accurate flood mapping is closely related to the description of channel geometry (Maidment, 1992). However, obtaining river geometry presents challenges. Indirect methods, such as the downstream hydraulic geometry (DHG) theory described by Leopold and Maddock (1953), use empirical power laws to estimate river geometry, including river width, depth, and velocity. Although this method is straightforward, it has certain limitations. Hydraulic geometry parameters are often uncertain or difficult to spatialize (Andreadis et al., 2013). In contrast, conventional hydrodynamic or low-complexity models estimate the geometry by linking it to floodplain delineation (Afshari et al., 2018).

Conventional hydrodynamic models are primarily physically based, and delineate flooding by incorporating channel geometry, including cross-sectional shape, surface roughness, and hydraulic structures (Bates and De Roo, 2000; Kim et al., 2011; Musser and Dyar, 2007; Tayefi et al., 2007). However, the number of inputs required to execute these models limits their applicability. On the other hand, low-complexity models use available data such as DEMs and land cover maps to delineate floodplains over extensive areas (Jafarzadegan et al., 2018; Samela et al., 2017; Sangwan and Merwade, 2015).

As a simplified approach, HAND normalizes elevation differences in the DEM to estimate floodplain extent (Nobre et al., 2011; Rennó et al., 2008). HAND relates river geometry, stage, and discharge via SRCs. Consequently, hydraulic parameters derived from channel shapes (Quintero et al., 2021; Zheng et al., 2018) enable the creation of first-instance flood maps. Although HAND simplifies complex physical processes, its computational efficiency enables flood mapping in data-scarce areas, despite inherent uncertainties (McGrath et al., 2018; Teng et al., 2017). In addition, as a zero-dimensional model, HAND-SRC does not account for the spatial and temporal variability of rainfall and runoff, thereby influencing both flood extent and duration (Johnson et al., 2019). Furthermore, it lacks the capability to depict intricate hydrodynamic processes including backwater effects, hydraulic structures, and channel geometry (Chaudhuri et al., 2021). Finally, changes in land use and climate are not substantially reflected in their impact on flood risk mapping. In summary, this method is suitable for preliminary flood documentation when dealing with open-channel flows, assuming that the geometric properties established through LiDAR analysis remain valid during flood events. This explicitly excludes ice-jam floods, which are associated with a reduction in flow areas.

Although the HAND-SRC approach has been applied to large watersheds (Diehl et al., 2021; Garousi-Nejad et al., 2019; McGrath et al., 2018; Scriven et al., 2021; Zheng et al., 2018), uncertainties persist regarding its effectiveness and accuracy for small watersheds. These uncertainties include the resolution of the DEM and the topography. Moreover, previous studies have demonstrated that high resolution DEMs can provide a more accurate representation of channel geometry and improve flood mapping (Garousi-Nejad et al., 2019; Rebolho et al., 2018) Prior research projects have highlighted the importance of DEM resolution, as it directly affects the shape and distribution of elevations. Additionally, it has been observed that changes in reach length and slope can negatively impact the performance of the SRC, leading to overestimations of floodplains, especially in low relief areas like agricultural regions(Godbout et al., 2019).

In addition to topographic factors, the Manning roughness coefficient is another source of uncertainty in the SRC performance. Fernandes (2021) incorporated shear stress at the channel-floodplain interface to correct this coefficient, resulting in improved prediction of overbank flow. Another way to enhance the accuracy of SRC is by using weighted Manning values derived from land cover maps, considering both minimum and average values (Scriven et al., 2021). Furthermore, Gomes et al. (2023) found that using a single roughness coefficient can lead to an overestimation of conveyance with up to 30% for in-bank flows and 100% for large overbank flows. These findings highlight the physical implications associated with estimating the Manning roughness coefficient. Finally, Ghanghas et al. (2022) emphasized the importance of modelling assumptions as another significant source of uncertainty, in addition to topographic factors. Despite some exclusions such as bathymetry, the HAND-SRC method can still provide consistent rating curves over large areas, even though uncertainties may persist. All the studies underscore the importance of considering and quantifying sources of uncertainty, along with topographic factors when approaching flood mapping.

Furthermore, combining SRC with HAND data poses challenges in acquiring accurate topographic data through remote sensing. However, the upcoming Surface Water and Ocean Topography (SWOT) mission may present an opportunity (Biancamaria et al., 2010). SWOT provides water surface elevation and extent data that can support the HAND values. Combining SWOT observations with HAND-derived flood modeling would enable enhanced flood forecasting and improve the understanding of water dynamics and climate change impacts. However, it is important to note that SWOT does not directly measure slopes, discharges, or network topologies (Biancamaria et al., 2016). Therefore, integrating SWOT with DEMs and hydrologic modeling will be necessary for flood delineation using SRC and HAND.

Nevertheless, based on previous studies, it is possible to identify five critical tasks that could reduce uncertainties: (i) improving the resolution of the DEM, (ii) evaluating the vertical accuracy of LiDAR data, (iii) examining the effects of the Manning coefficient on discharge, (iv) assessing the impacts of reach length, and (v) validating the influences of channel morphology on floodplain mapping. By addressing these tasks, the accuracy of the HAND-SRC for floodplain delineation would be enhanced. Furthermore, these tasks represent a novel approach.

2. Material and methods

The methodology described herein consists of five stages for the setup, application, and validation of the HAND-SRC method in small watersheds: (i) identifying the study area and retrieving available hydrological datasets, (ii) applying the HAND method and

deriving SRCs to delineate inundated areas by comparing them with a historical flood, (iii) performing a Global Sensitivity Analysis, (iv) selecting the best SRC based on observations, and finally (v) computing and locating hydraulic benchmarks to strengthen the results.

2.1. Study area

The methodology was implemented on two pilot watersheds in Quebec, Canada, as shown in Fig. 1. The first is the St. Charles River watershed, located in a mixed urban-rural region on the north shore of the St. Lawrence River near Québec City. It drains a 554 km^2 region and has six main tributaries. The average precipitation in this region is 1287 mm/year. The second is the À la Raquette River watershed, primarily an agricultural region draining 133 km^2 and situated west of Montreal. The average precipitation in this region is 998 mm/year. These watersheds were selected based on their size, number of hydrometric stations, and the spatial resolution of the available DEMs. The Water Expertise Center of Québec (CEHQ) operates the hydrometric stations of the St. Charles River watershed, while the Université du Québec À Montréal (UQÀM) operates the hydrometric stations of the À La Raquette River watersheds.

2.1.1. Input geographic datasets

2-m DEMs were created using airborne Light Detection and Ranging (LiDAR) data obtained from the *Communauté Métropolitaine de Montréal* and *Communauté Métropolitaine de Québec* for the À La Raquette and St. Charles River watersheds, respectively (MFFP, 2020). The LiDAR data was calibrated using the Can-Net network and all available geodetic points (MERN, 2021). The DEMs utilize the GRS 80 reference ellipsoid with the NAD 83 SCRS geodetic reference system and a Modified Transverse Mercator (MTM) projection. A river network map at a scale of 1:20.000 was retrieved from the Quebec Hydrographic Network GeoBase (QRHM), which is available from

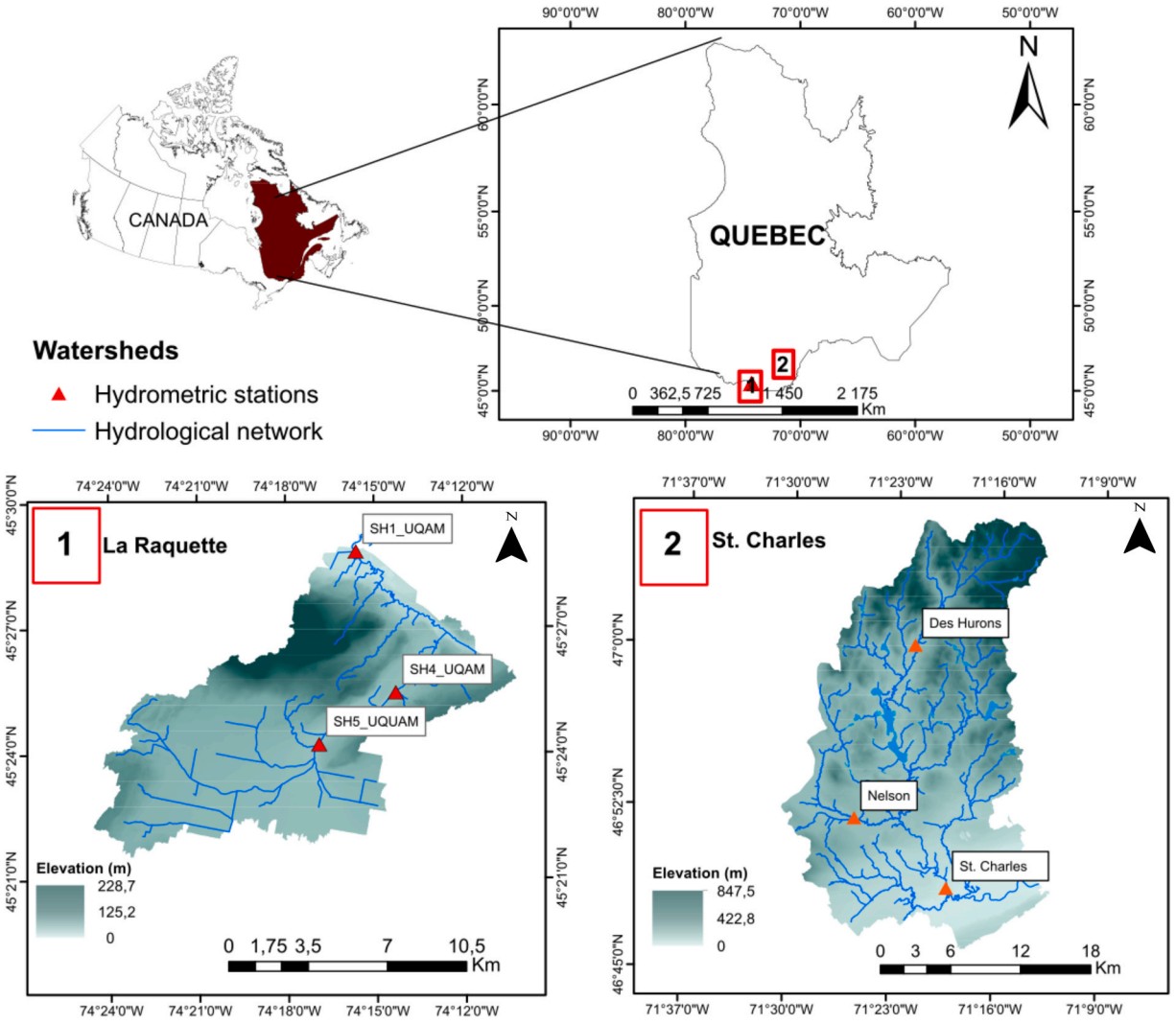

Fig. 1. À la Raquette and St. Charles watersheds, including the location of their gauge stations and river network.

the Quebec Ministry of Energy and Natural Resources website (MERN, 2022). Land cover maps, derived from the analysis of aerial imagery, were obtained from the Quebec Ministry of Environment and Fight against Climate Change at a spatial resolution of 10 m. The dataset used in this study aligns with maps produced in 2019 (MELCC, 2019).

To improve the accuracy of the hydrographic network, the river reach connectivity was fine-tuned to remove loops and segments with multiple outlets. Table 1. presents an overview of the different land cover categories within both watersheds. The percentages were calculated by dividing the area of each specific land cover type by the total area of the respective watersheds. It is worth noting that the St. Charles watershed has a higher proportion of forest and urban land cover compared to the predominantly agricultural land cover observed in the À la Raquette River watershed.

2.1.2. SRCs and HAND modelling

The derivation of SRCs from a HAND matrix was based on the methodology proposed by Zheng et al. (2018) and the equations for calculating channel hydraulic properties based on elevation and hydrographic data. The geometric properties of a river reach include the wetted perimeter, hydraulic radius, volume, and width of the inundated area. Fig. 2 shows the proposed methodology for deriving SRCs. To demonstrate the potential of this method for floodplain mapping, SRCs are used to provide the corresponding water level for a given discharge provided by HYDROTEL. HYDROTEL is a process-based, continuous, and semi-distributed hydrological model that requires the delineation of a watershed into "Relatively Homogeneous Hydrological (i.e. hillslopes) Units" (RHHU) and river segments (Bouda et al., 2014; Bouda et al., 2012; Fortin et al., 2001; Turcotte et al., 2007; Turcotte et al., 2003). HYDROTEL relies on PHYSITEL (Noël et al., 2014; Rousseau et al., 2011; Turcotte et al., 2019) for the watershed discretization. This hydrological model was chosen for its versatility and the fact that the HAND-SRC framework had already been implemented as a submodule of PHYSITEL/HYDROTEL modelling (see the following section).

2.2. HAND

A 64-bit version of PHYSITEL, a Geographic Information System (GIS) developed to support the implementation of distributed hydrological models, was used to analyze the terrain data and produce the HAND matrix (Noël et al., 2014; Rousseau et al., 2011; Turcotte et al., 2019). Within PHYSITEL, users can modify river and lake connectivity while performing various calculations such as determining DEM cell slopes, directions, and accumulation. Additionally, as mentioned earlier, the GIS delineates watersheds into (RHHUs), specifically categorizing them as hillslopes.

The main calculations used to obtain the HAND matrix correspond to the methodology described by Nobre et al. (2011). However, the module available in PHYSITEL includes several modifications. Among these modifications is the possibility of adjusting Manning roughness coefficients based on the values reported in Chow (1959). This allows the modification of the coefficients according to varying land cover. Additionally, the length of the river reach can be tailored to the channel width. This adjustment is based on the USGS recommendations included in the manual of Rantz (1982) for installing a hydrometric station along a homogeneous reach (i.e., segment).

To execute HAND, the cells (i.e., pixels) corresponding to the river network were set to an elevation of 0. Subsequently, the vertical differences between the terrain pixels and hydrographic network pixels were calculated using the flow orientation matrix and pixel elevations. The HAND conceptual approach delineates the inundated area through an iterative process using Eq. (1). Any pixel with a water level higher than its HAND value was considered inundated.

$$if \quad y > h(s) = inundated \quad pixel \tag{1}$$

Where $h(s)$ [m] or HAND value is the difference between the elevation of the cell s and the minimum channel elevation of the corresponding stream where water drains, and y [m] is the average water level within reach.

2.2.1. Hydraulic geometry

Channel geometry is determined by averaging longitudinal cross-sections (i.e., slices) taken along the length of the channel, rather than dividing the flow path into cross-sections. Additionally, Zheng et al. (2018) demonstrated that hydraulic simulations using the Manning equation could be conducted using hydraulic geometric properties derived from a DEM. These properties depict the channel shape as shown in Fig. 3. Hydraulic parameters were utilized to establish the foundation for calculating a SRC.

The model delineates the inundated zone $F(y)$ by identifying the cells s whose water level y is greater than the HAND value $h(y)$. Thus, the water depth $d(s)$ at any cell s is the difference between the reach average water level y and the HAND value of that cell $h(s)$, as

Table 1
Land cover distribution (%) in À La Raquette River and St. Charles watersheds based on aerial imagery analysis.

Land cover	*St. Charles*	*À la Raquette*
Forest	61%	42%
Wetlands	6%	3%
Urban areas	27%	2%
Agriculture	3%	52%
Bare soil	2%	1%

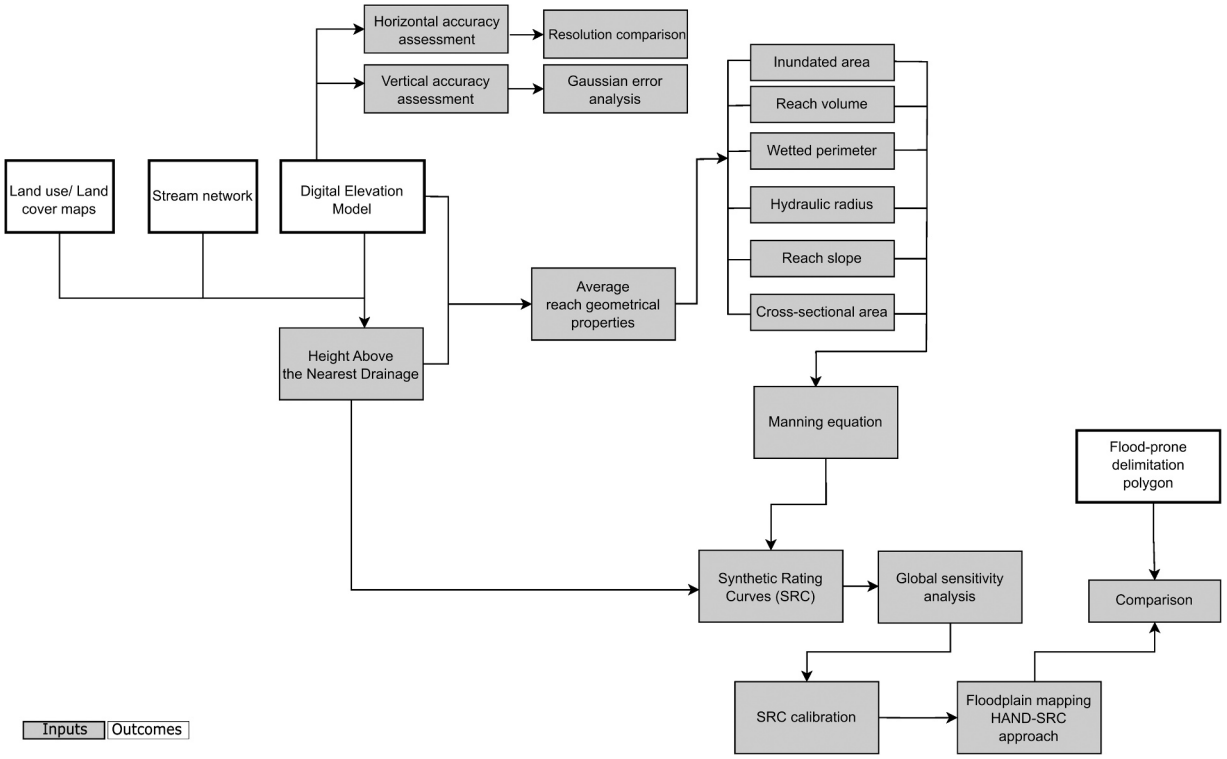

Fig. 2. Flow chart of the proposed approach for generating SRC and first-instance floodplain maps in small watersheds.

represented in Eq. (2):

$$d(s,y) = y - h(s), s \in F(y) \tag{2}$$

The Manning equation assumes steady and uniform turbulent flow, although this assumption may not be valid for all reaches. However, the uncertainty related to this assumption can be quantified through hydraulic parameter validation. In most practical applications, the hysteresis phenomena where the stage is lower during the rising limb than on the recession limb of the flood-wave hydrograph, is generally considered negligible (Henderson, 1966). Nevertheless, periodic validation and updating of the equilibrium rating curve are necessary due to geomorphological changes over time caused by bank erosion and sedimentation (Chow et al., 1988).

Additionally, the calculated values of the hydraulic geometry parameters can be compared with those obtained from the Hydrologic Engineering Center's River Analysis System (HEC-RAS). HEC-RAS is a tool used for deriving channel geometry, particularly when data is readily available. This comparison is especially important for parameters linked to the minimum elevations of the riverbed, as they tend to be the most uncertain values.

The HAND implementation in PHYSITEL was established using Eqs. (3–8), which were defined for a uniform average reach at water level *y*. The symbols and units used in the subsequent sections are summarized in Table 2. The following parameters are computed: the inundated surface *S(y)*, channel bed area *B(y)*, flooded area volume *V(y)*, average cross-sectional area *A(y)*, wetted perimeter *P(y)*, and hydraulic radius *R(y)*.

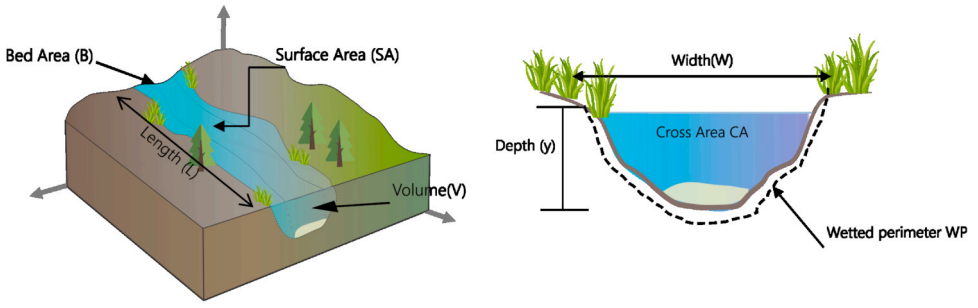

Fig. 3. Illustration of the cross-section and the longitudinal hydraulic geometric properties derived for each river reach.

$$S(y) = n\,A(s) \tag{3}$$

Where n is the number of inundated cells within the reach, and $A(s)$ is the area of the cell s.

$$B(y) = \sum\nolimits_{s \in F(y)} A(s)\sqrt{(1 + slp \quad (s)^2)} \tag{4}$$

Where *slp (s)* refers to the slope of each cell and is calculated as the inverse tangent of the slope angle.

$$V(y) = \sum\nolimits_{s \in F(y)} A(s)d \quad (s, y) \tag{5}$$

$$A(y) = \frac{V(y)}{L} \tag{6}$$

$$P(y) = \frac{B(y)}{L} \tag{7}$$

$$R(y) = \frac{A(y)}{P(y)} \tag{8}$$

Once the river channel geometry and Manning roughness coefficient have been defined, the Manning equation, (Eq. 9) is applied to estimate the discharge for each river reach, given the water level (y). Finally, the model calculates the discharge from the bottom to the flood height by gradually increasing the water level. As a result, a stage-discharge relationship known as SRC is derived for each river reach within the watershed. The hydraulic parameters obtained from this approach are solely based on geometric attributes extracted from gridded data, providing an average representation of river reaches, and capturing sufficient data for the computation of the Manning equation. Although this approach does not consider river bathymetric data, we propose an alternative procedure to correct LiDAR data *using* in situ rating curves in Section 2.2.3.

$$Q(y) = \frac{1}{n} \quad AR^{\frac{2}{3}}S^{\frac{1}{2}} \tag{9}$$

Where A refers to the cross-sectional area (m^2), R is the wetted perimeter (m), S is the channel slope (m/m), n is the roughness coefficient, and $Q(y)$ is the discharge (m^3/s).

Floodplains can include multiple land-cover types, each associated with different roughness coefficients. To enhance the accuracy of SRC, the use of a composite n value has been suggested by Garousi-Nejad et al. (2019); Scriven et al. (2021) and Zheng et al. (2018). This composite value is determined based on the weighted perimeter of each land cover type at the reach scale, as explained by Crosato et al. (2020). However, the uncertainty surrounding the floodplain n value remains in this study. Additionally, while there are multiple equations available to calculate the weighted value of n, this study adopts the equivalent roughness coefficient proposed by Einstein (1934) and Horton (1933) in the GIS PHYSITEL, as presented in Eq. (10). The resulting n value represents an equivalent value that considers the perimeters of each subsection based on the land cover.

$$n_{eq} = \left[\frac{\sum_{i=1}^{n} p_i n_i^{\frac{3}{2}}}{P}\right]^{\frac{2}{3}} \tag{10}$$

Where n_i is the Manning coefficient of land cover i, P_i is the wetted perimeter of land cover i, and P is the total perimeter.

2.2.2. Rating curve comparison

A comparison was made between the derived SRC using PHYSITEL and the hydrometric data from six gauging stations. The

Table 2
Symbols and units.

Variable	Symbol	Units
Inundated surface	$S(y)$	m^2
Area of cell s	$A(s)$	m^2
Channel bed area	$B(y)$	m^2
Pixel Slope	*slp*	$m.m^{-1}$
Volume	$V(y)$	m^3
Length	L	m
Wetted perimeter	$P(y)$	m
Hydraulic radius	$R(y)$	m
Manning roughness coefficient	n	$m^{1/3}s^{-1}$
Discharge	$Q(y)$	m^3s^{-1}
Cross-sectional area	$A(y)$	m^2
Reach slope	S	$m.m^{-1}$

comparison involved several steps. First, the geospatial reference system was corrected to ensure compatibility between the two datasets. This involved modifying the “official” rating curves to fit the benchmark reference system into a geodetic reference system. Specifically, the NAD 83-CSRS reference system was used for the À La Raquette River, and UTM 18 N and UTM 19 N projections were used for the St. Charles River watersheds. The altimetric reference system CGVD28 was also utilized. In situ positioning was then performed using Leica’s Real-Time Kinematic (RTK) method with GNSS-RTK GS08 Plus. Two goodness-of-fit indicators were applied to assess the difference between the observed and synthetic rating curves. These indicators were the Root Mean Squared Error (RMSE) (Eq. 11a), the Normalized RMSE (Eq. (11b), and the percentage of bias (PBIAS, Eq. 12) introduced by Yapo et al. (1996). The comparison was conducted at a river reach near the gauge station to ensure that both curves had the same coordinate system and represented an equivalent channel morphology.

$$RMSE\left(m^3/s\right) = \sqrt{\frac{\sum_{i=1}^{n}(Q_0 - Q_s)^2}{N}} \tag{11a}$$

$$NRMSE = \frac{RMSE}{\overline{Q_o}} \tag{11b}$$

$$BIAS \quad (\%) = \left[\frac{\sum_{i=1}^{n}(Q_0 - Q_s) * 100}{\sum_{i=1}^{n} Q_0}\right] \tag{12}$$

Where Q_o corresponds to the observed discharge, Q_S is the simulated discharge and $\overline{Q_o}$ is the average of the observed discharges; all values in (m^3/s).

2.2.3. Resolution effect

The term "resolution" encompasses more than just pixel size. Resolution refers to the model’s ability to distinguish objects and is linked to the smallest wavelength needed to detect shapes (Polidori and El Hage, 2020). On the other hand, pixel size refers to the size of the grid, and some researchers use "pixel" to describe the technology while using "grid" to refer to the model (Hengl, 2006). Previous studies have demonstrated that the accuracy of HAND can be improved by using high-resolution gridded data due to the nature of resolution. Higher resolution allows HAND to better delineate terrain features, such as channels and floodplains which are critical for flood modeling. Therefore, higher resolution directly enhances the performance of HAND in terms of object discrimination. Additionally, applying this model could stimulate efforts to gather hydrological information in areas with limited data. Furthermore, the absence of bathymetric data was assessed considering that LiDAR data was collected during the low-flow season and that the land cover of the floodplain was more significant than that of the channel. The DEM serves as the primary data source for the HAND model. To examine the impact of resolution on SRC derivation, two approaches were implemented.

2.2.3.1. Vertical accuracy. The vertical accuracy of DEMs is related to their ability to accurately represent surfaces, specifically how realistic their shape appears. DEM errors can arise from various sources, including input data, processing methods, and scale influence (Polidori and El Hage, 2020). However, research has shown that DEM errors typically follow a Gaussian function (Heuvelink, 1998). In Fig. 4, a bias is depicted between the modelled surface and the ground truth, known as systematic error. This bias can be influenced by the production technique and data interpolation methods. On the other hand, random errors are primarily caused by the production techniques and depend on factors such as the quality of the raw data, processing parameters, terrain morphology, and vegetation. These errors can be assessed by calculating the standard deviation of the elevation difference. Lastly, gross errors are outliers that result from errors during the production of the DEM (Polidori and El Hage, 2020). By considering that a normal distribution can represent the propagation of errors, the effect of vertical accuracy can be analyzed using the confidence intervals $[\mu - \sigma, \mu + \sigma]$ of the function described in Eq. 13.

$$f\left(x \quad | \quad \mu, \sigma^2\right) = \frac{1}{\sigma}\varphi\left(\frac{x - \mu}{\sigma}\right) \tag{13}$$

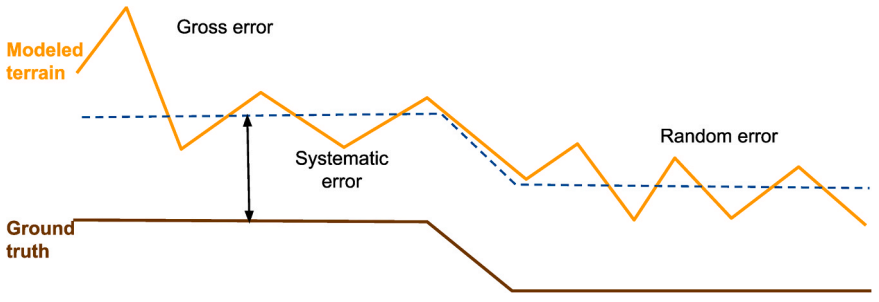

Fig. 4. Behavior of the vertical accuracy of DEMs.
adapted from (Polidori et al., 2020).

Where μ corresponds to the mean and σ is the standard deviation of the data.

To assess the vertical accuracy of the DEM, a new DEM was generated to incorporate a systematic error. This modified raster was used as input for analyzing the impact of normally distributed errors on the SRC, as shown in Fig. 5. Additionally, using Data Analysis Tools, a normally distributed random error with a standard deviation of ± 15 cm was introduced into a new DEM. This value, chosen based on the LiDAR metadata accuracy, allowed for the assessment of vertical accuracy impacts.

Furthermore, one of the gauge stations was selected to carry out the HAND-SRC method using the modified DEM. The purpose of this analysis was to assess sensitivity of the model to potential errors when utilizing LiDAR data.

2.2.3.2. Horizontal Resolution. The second approach in assessing DEM errors examined how the accuracy of SRCs could be improved by increasing the spatial resolution of the DEM. The DEMs were upscaled to different horizontal resolutions of 5 m, 4 m, 3 m, and 2 m. A MATLAB script was developed to generate a series of rating curves for each gauge station at various resolutions. Using high-resolution data allowed us to examine the impact of resolution on the results and associated computational costs. The effect of changing the grid size on the horizontal resolution was also evaluated, and performance metrics such as RMSE and BIAS were employed to measure this impact.

Uncertainties affect model calibration and validation. Sensitivity analysis quantifies the influence of parameters on model response, assisting in uncertainty analysis (Pianosi and Wagener, 2016). In this study, a global sensitivity analysis (GSA) was conducted, considering each forcing parameter.

2.2.4. Classification assessment

To quantify the error between the flooded area derived from historical discharge and the one obtained through simulated discharge and HAND-SRC, a confusion matrix and performance metrics such as precision, overall accuracy, F1 score, recall, and Intersection Over Union (IoU) were calculated for each parameter combination.

The confusion matrix enables the classification of the simulation results in relation to the ground truth image, which represents the polygon of regulated risk zones. Therefore, the overall accuracy (OA) Eq. (14) is determined as follows:

$$OA = \frac{TP + TN}{N} \tag{14}$$

Where *TP* is the total number of correctly classified pixels for the positive samples, *TN* is the total number of correctly classified pixels for the negative samples, and *N* is the total number of samples. The recall, precision, F1-score, and intersection over union (IoU) Eqs. (15–18) are determined as follows:

$$Recall = \frac{TP}{TP + FN} \tag{15}$$

$$Precision = \frac{TP}{TP + FP} \tag{16}$$

$$F1_{score} = \frac{2 \cdot Precision \cdot Recall}{Precision + Recall} \tag{17}$$

$$IoU = \frac{TP}{TP + FN + FP} \tag{18}$$

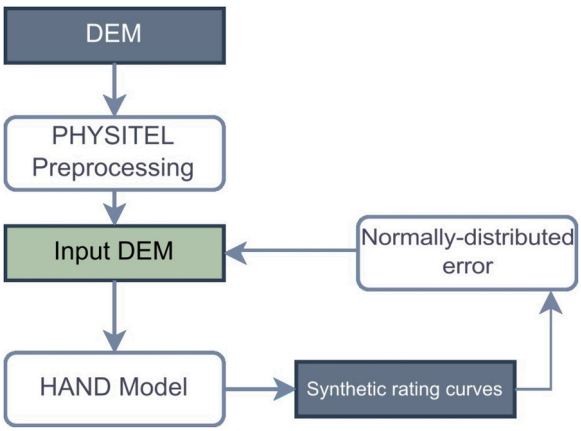

Fig. 5. General workflow for vertical accuracy assessment.

Where *FP* represents the total number of incorrectly classified pixels for the negative samples, *FN* represents the total number of incorrectly classified pixels for the positive samples, and *TN* represents the total number of correctly classified pixels for the negative samples.

2.3. Global sensitivity analysis

A sensitivity analysis (SA) provides information on how changes in parameter values can influence modelling results. Sensitivity analyses can be divided into two main groups: local (LSA) and global (GSA). Local approaches involve varying the values of input parameters within a range of pre-calibrated optimum values. In contrast, GSAs involve varying input parameters across a wide range of values to reflect the uncertainty estimation of each factor (Pianosi et al., 2015). In this study, the Variogram Analysis of the Response Surfaces (VARS) method (Razavi and Gupta, 2016a) was used to conduct the (GSA) of the HAND-SRC methodology. Specifically, the GSA focused on the Manning roughness coefficient and the length of the river reach as the key input parameters. VARS was chosen as the preferred approach for this analysis. Finally, the effect of each parameter was quantified by considering their associated errors, thus optimizing the calibration process (Savage et al., 2016).

2.3.1. VARS framework

The VARS framework is a GSA based on the theory of response variograms. The model is theoretically based on the sensitivity definition of directional variograms and co-variograms. The framework offers several advantages, including ease of implementation, low computational cost, and the ability to compare sensitivity based on three different indicators: Sobol (Sobol‴, 2001), Morris (Morris, 1991), and IVARS. IVARS, which stands for Integrated Variogram Across a Range of Scales is a perturbation scale in the factor space that measures the rate of change in the model response. It provides a series of sensitivity metrics for the VARS model. Compared to other approaches, VARS provides statistical robustness, high efficiency, and stability (Razavi and Gupta, 2016a).

The factor space in the VARS framework is delimited by the upper and lower physical limits of the parameters. The sampling strategy in the framework is based on the STAR methodology developed by Razavi and Gupta (2016b). This strategy allows for the computation of the full sensitivity range and reduces numerical costs. Once the input file is defined using the factor space, the model runs with each new input combination. The framework then provides an output file that is analyzed to calculate the sensitivity metrics.

2.3.2. Manning roughness coefficients

Manning roughness coefficients can vary depending on the flow medium (Chow, 1959). In this study, three categories of coefficients were used to group similar surface flow media: (i) Channel, (ii) Forest, and (iii) Other. The “Other” category includes terrain pixels that were not included in the first two categories. The GSA implementation was based on values reported by Chow (1959) and commonly used in distributed hydrological modelling, such as those provided by HYDROTEL (Bouda et al., 2014; Bouda et al., 2012; Fortin et al., 2001; Turcotte et al., 2007; Turcotte et al., 2003), for which PHYSITEL was developed. Therefore, a range of variations was established to validate the methodology. The minimum and maximum values of the input parameters are presented in Table 3.

2.3.3. Reach length

Determining the reach length, a critical parameter in HAND-SRC modelling, is paramount as it can significantly affect the accuracy of the results. In this study, the reach length was carefully selected to ensure reliability and consistency with real-world conditions. To achieve this, the guidelines provided by the USGS for the installation of gauge stations were used, which recommend fixing the reach length (Rantz, 1982). Additionally, to ensure that the reach length corroborated with the river’s natural course and as suggested by Richardson et al. (2017), the length was set to be seven times the river width. By adhering to this criterion, the model is expected to accurately simulate real-world scenarios. The resulting SRCs can be compared with those obtained from gauge station data, providing a reliable and robust measure of representativity. Finally, following the calibration process, a comprehensive comparison was conducted to validate the optimal ranges of rating curves for reach lengths ranging from 50 to 300 m. These comparisons aimed to determine the general ranges within which the optimal rating curves could be identified and applied effectively.

2.4. Calibration and river reach selection

2.4.1. Calibration: Selection of the best rating curves

The sampling strategy from VARS provided a dataset of 4600 new sets of input parameters. This dataset sorted the parameter sensitivities according to the VARS framework. However, this sample data also tracked the values of the input parameters that produced accurate SRCs. To retain the curves that match the observed rating curve of each gauge station, a filter based on the absolute PBIAS of $\pm$ 20% was applied. This process resulted in an envelope of “representative curves”. Then, a Hit/Miss score criterion was

Table 3
Manning roughness (n) coefficient limits.

Land cover n	Lower limit	Upper limit
Forest ($m^{1/3}/s$)	0.03	0.3
Channel ($m^{1/3}/s$)	0.015	0.15
Other land cover ($m^{1/3}/s$)	0.025	0.25

tested to extract the curves that fell within a ± 5% range of each point on the observed rating curve. This range is often recognized as their general accuracy (Pelletier, 1988). A "hit" score was assigned to a point on the curve if it fell within the mentioned range; otherwise, it was assigned a "miss" score. Thus, each point of the SRC was compared to the observed curve. Only curves with a "hit" score greater than or equal to 65% were kept. This percentage ensured that a minimum number of curves (at least ten for each station) was achieved.

2.4.2. Topomorphologic criteria of steady uniform flow

River regimes are typically turbulent, and they can be classified as either subcritical or supercritical, depending on whether gravitational or inertial forces prevail. This classification is characterized by the Froude number (see Eq. 19). After the calibration process, the required information to calculate the Froude number was extracted from the hydraulic geometry properties, which were determined using the gridded elevation data described previously.

$$Fr = \frac{v}{\sqrt{gD_h}} \tag{19}$$

Where v is the average velocity in the channel [m/s], g is the acceleration due to gravity [m.s^{-2}], and D_h is the hydraulic depth [m]; that is for the HAND-SRC approach, the ratio of the average cross-sectional area $A(y)$ over the top width of the flow $W(y)$. The latter is defined as follows: $W(y) = S(y)/L$.

The modelling framework involves using the SRC relationship between hydraulic depth and average velocity of a river reach. However, the semi-empirical Chézy Eq. (20) demonstrates that this relationship is not univocal. In other words, there can be two matching velocities for a given hydraulic depth, corresponding to the subcritical and supercritical turbulent flow regimes. Therefore, Froude numbers were calculated for all river reaches using realistic discharge values (based on the discharge-area relationship). These Froude numbers were used as a basis for excluding any river reach where the flow regime changes with discharge.

$$v = C\sqrt{R.J} \tag{20}$$

Where v is the mean velocity [m/s], C is the Chézy resistance coefficient [m$^{1/2}$/s], R the hydraulic radius [m], and J the energy gradient [m/m].

Manning derived an empirical equation for the Chézy coefficient:

$$C = 1/n \quad R^{\frac{1}{6}} \tag{21}$$

Where C *is* the form of the Chézy coefficient according to Manning-Strickler [m$^{1/2}$/s], n is the Manning roughness coefficient [s/m$^{1/3}$], and R is the hydraulic radius [m]. This is one of the most commonly used forms and is considered a good approximation of real-world conditions. Its use implies that the gravitational force in the direction of flow is balanced by the friction force (bed slope, energy grade line and water surface are all parallel). This requirement is met under steady uniform turbulent flow and non-steady gradually varied turbulent flow conditions, where the hydrostatic pressure and uniform mean velocity assumptions hold. However, for non-steady rapidly varied flow, these assumptions do not hold as wave dynamics need to be considered.

Generally, for bed slopes less than 10°, the friction slope is considered equal to the bed slope (Chow et al., 1988; Mays, 2005), and therefore the Manning equation can be used. To be conservative and consistent with the findings of Godbout et al. (2019) regarding extreme slopes, we excluded the application of the HAND-SRC modelling approach for river reach slopes exceeding 10% (a 10% slope corresponds to an angle of 5.7°).

Based on the Hit/Miss score, we identified the most accurate rating curves and their input parameters. We then applied the calibrated parameters to river reaches upstream of each gauge station. The regime unicity was calculated from the minimum and maximum discharge values observed at each station. The difference between the minimum and maximum values of discharges was divided into 10 intervals. For each interval the height, velocity, and Froude number for each river reach were calculated, and all non-compliant reaches were excluded.

3. Results

3.1. VARS model

As mentioned earlier, VARS calculated that 4600 samples would be necessary to assess the sensitivity of the response surface of the model. The results showed that a group of SRCs fitting the selection criteria can be obtained at each gauge station.

IVARS metrics sorted out the parameters in terms of their sensitivity, comparing them to other GSA approaches such as Sobol and Morris for each station. Table 4 introduces the results of the GSA. In terms of sensitivity, the reach length ranked first for four out of six stations. This result can be explained by the influence of the hydraulic geometric properties used in calculating the discharge. The results further emphasized the significance of the Manning coefficient in the channel of the St. Charles and Nelson stations. This finding was corroborated by the fieldwork, which revealed that both stations are situated within lengthy and homogeneous sections of the river. However, this result also reflects the different model behavior at each station, which motivated an independent calibration process. Similarly, the sensitivity analysis validated that the proximity between stations does not guarantee that their performance would be similar.

It is important to note that the results reflect what can be observed in the field. Both the St-Charles and Nelson gauge stations are located in river reaches that are much longer than the other stations, indicating their homogeneity. This is evident in the sensitivity behavior shown in Table 4 and demonstrates that our results are supported by in-situ observations.

3.2. Comparison with in-situ rating curves

SRCs were compared with those built using gauge station data. The first step involved using the default Manning roughness coefficients (0.1, 0.015, 0.04) for the different classes: forest, channel, and other, respectively, as taken from Chow (1959). Next, an analysis was conducted for the St. Charles River watershed to examine the impact of reach length on the accuracy of the resulting SRCs. Three gauge stations in the watershed exhibited differences in terms of river width: St. Charles River station (19.0 m), Nelson station (6.1 m), and Des Hurons station (7.2 m). Additionally, these stations had different local environments. Therefore, different combinations of Manning coefficient parameters were evaluated for each station, as well as three different lengths. Considering the similarity in terms of width, slope, and channel shape among the three stations in the À La Raquette River watershed, the comparison of reach lengths did not reveal significant differences in their behavior. Fig. 6 shows that a reach length of 50 m is not suitable for the St. Charles River station. This was expected, given its width of 19.0 m, which should be associated with a minimum reach length of approximately 140 m (refer to Section 2.3.3). When the reach length is below the theoretical value based on the river's width, it in inadequately represents the channel geometry, resulting in poorer performance. This result is significant as it demonstrates the alignment of our methodology's sensitivity with the guidelines proposed by the USDA. However, this length was appropriate for the remaining two stations. These results highlight the importance of the previously mentioned recommendations for installing a gauge station and the relationship between river width and the quality of the resulting SRCs.

The results of the validation exercise are presented in Table 5. The calibrated parameter values achieved the desired PBIAS ($\pm$ 20%) and had a hit score of at least 65%. In the case of the default values, the reach length corresponded to seven times the river width.

SRCs were normalized using Eq. (22), to identify the statistical trends in the results, considering the upper and lower limits defined in the factor space of VARS.

$$Norm_{parameter} = \frac{X_i - X\min}{X\max - X\min} \tag{22}$$

The solution space for the St. Charles River and À La Raquette River watersheds is depicted in Fig. 7. In the figure, the extremes of the radar plots represent the upper limits of the solution space, while the values closer to the intersection are related to the lower limits. This representation enables the identification of statistical trends associated with each station. Thus, it validates the necessity of the independent calibration at each station.

3.3. DEM resolution assessment

The analysis focused on the effect of systematic errors that arise from production techniques and data interpolation, as they can introduce bias. In addition, the use of high-resolution DEMs allowed for the assessment of the impact of horizontal resolution on SRC accuracy and computational costs. By varying the grid size, it was also possible to evaluate the effects of horizontal resolution on outcomes. Key performance metrics such as, NRMSE and PBIAS, were used to quantify these effects.

Fig. 8 displays the model performance when a systematic error is included. The "*n*" value corresponds to the number of rating curves used for the analysis. When comparing the results with the rating curve derived from in situ data for flows less than the maximum observed discharge, the PBIAS values vary from $-$ 10.75% to $-$ 25.96% and the NRMSE values vary from 0.46 up to 0.92. The input parameters for each gauge station were based on the values already calibrated in the previous step. In Fig. 9, we compared our approach for different horizontal resolutions. To ensure consistency, we randomly selected five curves within the range of $\pm$ 5% of PBIAS for all evaluated resolutions. As a result, hydraulic geometry properties improved, leading to a decrease in PBIAS from 11% to 5%. We conducted the same calibration process for each set of gridded elevation data, considering the desired PBIAS and Hit/Miss score. However, as the horizontal resolution increased, the computation times also increased by about 40% due to the building of the flow direction and HAND matrices, which required several hours of calculation. Nevertheless, obtaining high-resolution data remains challenging in many areas, and satisfactory results can still be achieved using coarser resolutions.

In addition, Fig. 9 reveals a deviation in the behavior of the Nelson station at 3 m when compared to other DEM resolutions. This variation could potentially be attributed to the manipulation of the DEM. The upscaling method has the potential to introduce DEM

Table 4
GSA results for St. Charles River and À la Raquette River watersheds. The first position corresponds to the most sensitive parameter according to VARS Tool.

Sensitivity ranking	UQAM 1	UQAM 4	UQAM 5	St Charles	Nelson	Des Hurons
1	Length	Length	Length	Manning channel	Manning channel	Length
2	Manning channel	Manning forest	Manning channel	Length	Length	Manning channel
3	Manning forest	Manning other	Manning other	Manning other	Manning other	Manning other
4	Manning other	Manning channel	Manning forest	Manning forest	Manning forest	Manning forest

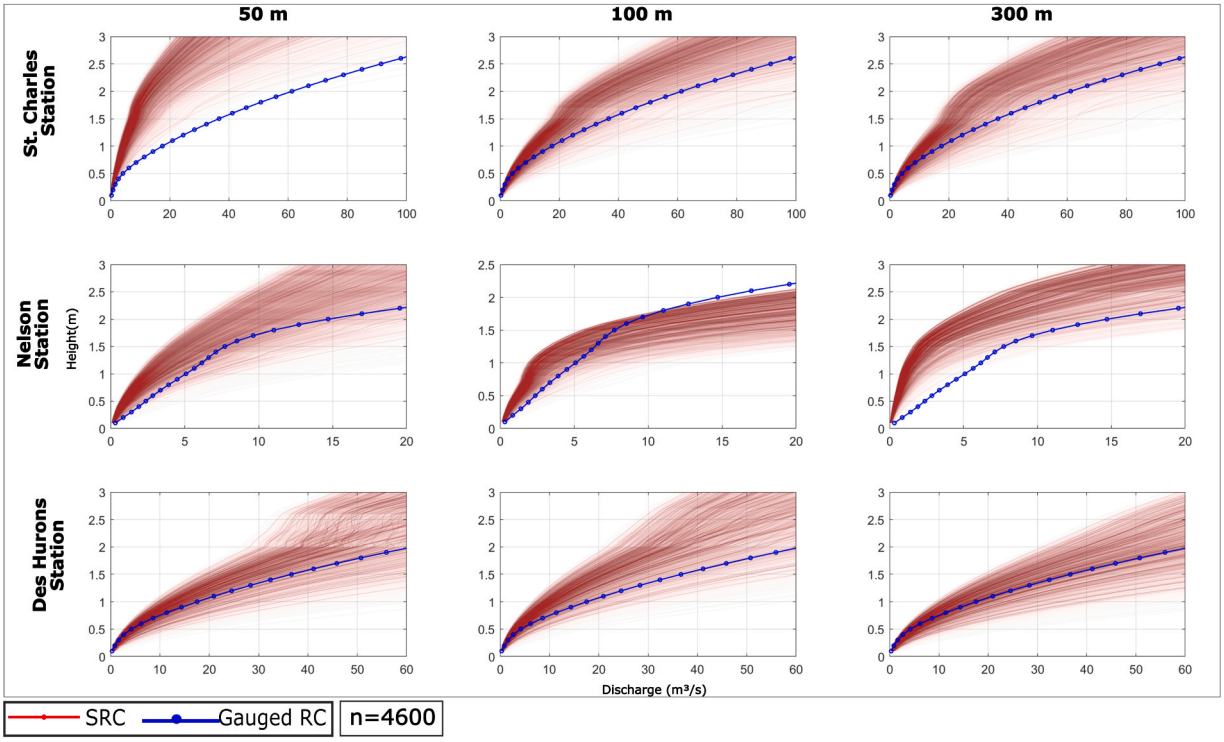

Fig. 6. Comparison of the river length in the St. Charles River watershed.

Table 5
Results of a so-called first approach HAND with default parameters and comparison those of the best rating curve based on % PBIAS.

Station	Number of curves	RMSE (m^3/s)		PBIAS (%)		Length (m)	
		Default	*Calibrated*	*Default*	*Calibrated*	*Default*	*Calibrated*
St. Charles	29	8.62	2.15	-16.36	-2.21	132.65	102.30
Nelson	23	5.42	0.53	-43.06	1.52	42.56	52.89
Des Hurons	12	24.36	0.74	-71.92	0.14	50.19	85.28
UQAM 1	14	22.51	0.98	26.25	-0.32	68.53	42.56
UQAM4	25	8.58	0.94	20.59	2.48	47.32	48.18
UQAM 5	30	2.66	0.57	-6.94	3.19	49.56	38.45

errors that can impact the overall outcomes, thus introducing errors into the analysis.

3.4. SRC calibration

After applying the criteria of ± 20% PBIAS, only a few SRCs were left for each station (at least 30 per station). This allowed for the analysis of input parameter trends at the watershed scale and the identification of unique parameter sets associated with selected gauge stations. An envelope was defined to obtain multiple sets of parameter values, and SRCs within ± 5% of the observed rating curve value (based on the hit or miss target) were selected. This methodology allowed for a more comprehensive analysis of parameter values and their effects on model performance.

An iterative estimation was applied to the SRC calibration to validate whether SRC calibration parameters could be used for the whole watershed. The results showed that for the À la Raquette River watershed, the selected sets of parameter values (i.e., values of the land cover Manning coefficients and reach length) could be applied at all three gauge stations and lead to SRCs falling within the range of ± 5% of PBIAS (see Fig. 10). On the other hand, the selected sets of parameter values need to be set independently to provide proper calibration. This aligns with what is observed in the field, where the areas around the stations and the average elevations are consistent for the À la Raquette River but notably distinct within the St-Charles River watershed.

The maximum recorded discharge value among the six stations is that of the St. Charles station, which is approximately ~78 m^3 /s. Based on this, a range of NRMSE values from 0.03 to 0.62 is considered acceptable for the six stations used to calibrate the SRCs. Despite the inherent uncertainties associated with the Manning roughness coefficients and a constant reach length, the HAND-SRC method shows promising results and certainly has the potential to be applied to small watersheds. Given the sought-after accuracy,

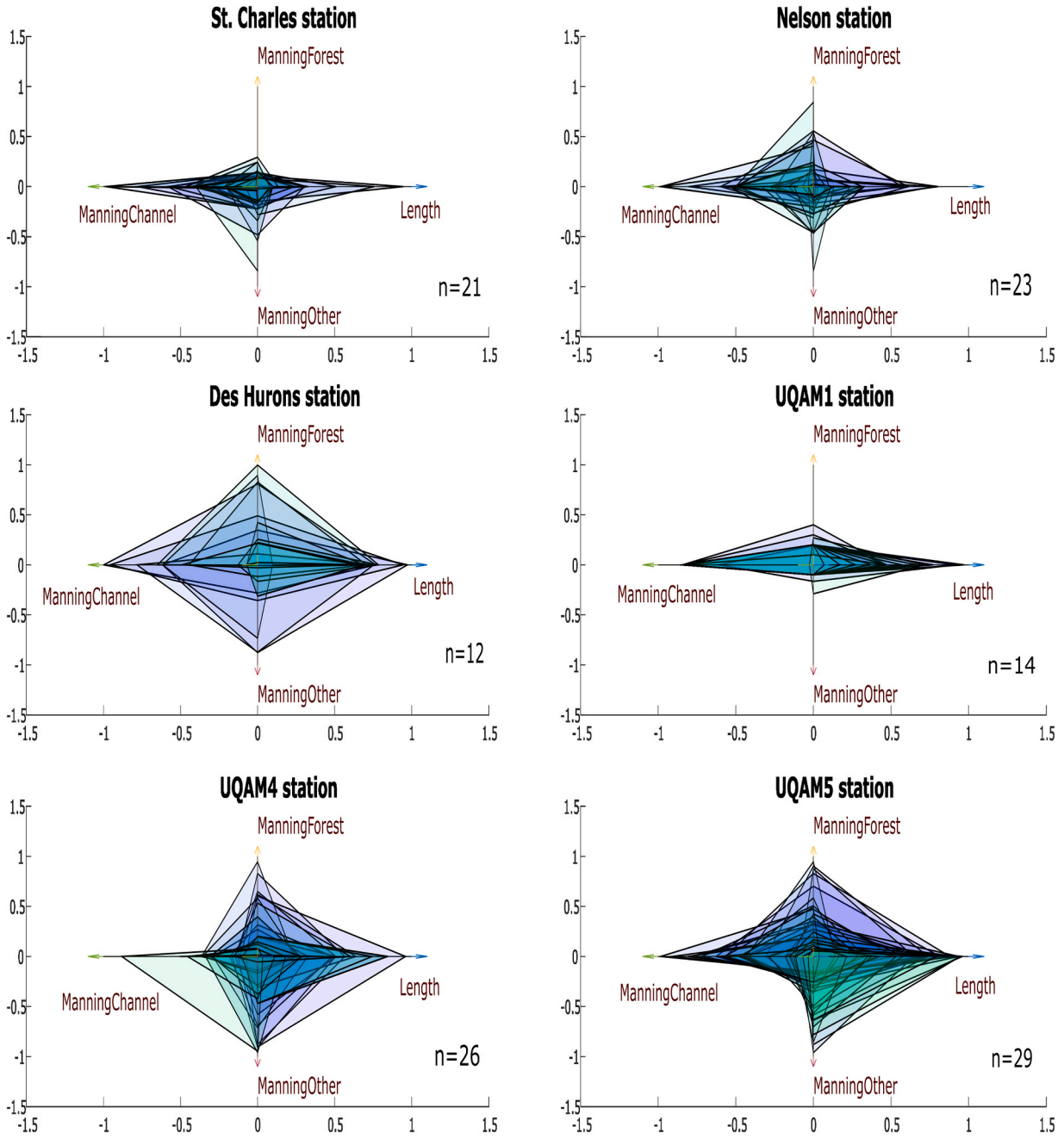

Fig. 7. The solution space for the St. Charles River and À La Raquette River watersheds was evaluated by examining the normalized performance of each (SRC) after the calibration process at the available gauge stations. The number of curves corresponds to the calibrated rating curves obtained using the HAND-SRC method. The normalized values indicate the most sensitive parameters identified through the (GSA) at each station. Darker colors indicate more superpositions of the factor space of the different sets of parameters than lighter tones.

it is first and foremost preferable to obtain a calibrated SRC for each gauge station rather than transferring a calibrated set of parameter values to other gauge stations.

3.5. River reach selection

Given the threshold of 10% for the river reach slope, a preliminary analysis was conducted to calculate the slope of each reach. This analysis was based on the assumption that a slope within this range ensures the applicability of the Manning equation, which requires the bed slope, energy grade line and water surface elevation profile to be parallel. The results of this slope classification for both the À

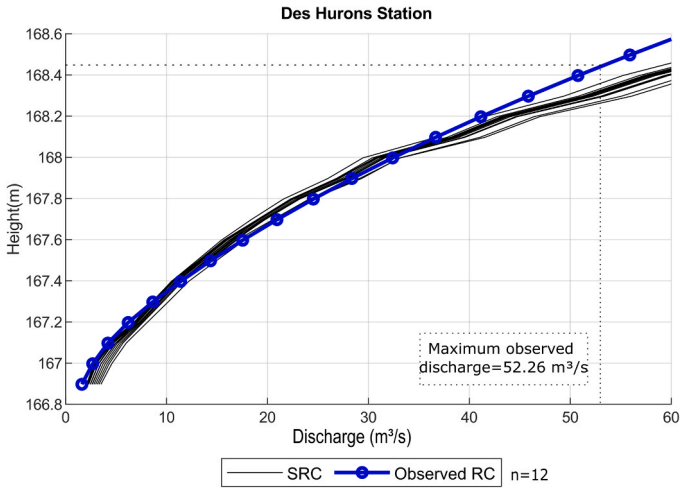

Fig. 8. Resulting SRCs using a DEM including a Gaussian error for the Des Hurons station.

La Raquette and St. Charles River watersheds are shown in Fig. 11, using a 2 m DEM resolution. In the St. Charles River watershed, 84% of the river reaches have slopes between 0% and 5%, while in the À La Raquette River watershed, 95% of the river reaches have slopes within this range.

In Fig. 12(a) and (b), different shades of red and purple indicate the bed slopes where the HAND-SRC results may be less certain and should be used with caution. Slopes exceeding 10% were excluded from the HAND-SRC results to ensure uniform flow and uniqueness of the flow regime, as shown in Fig. 12 (c) and (d). A region labeled as the "not recommended range" was then delineated based on the slope values. While analyzing the slope of each river reach could serve as a criterion for directly applying the HAND-SRC approach, an additional validation can be performed using the Froude number (*Fr*) to assess the hydraulic regime. River reaches that do not meet the requirement for flow regime uniqueness for more than 80% of their physically plausible discharges (determined from the maximum observed values at gauge stations and the drainage areas of each gauge station) were excluded from the HAND-SRC results.

This approach covered the range from subcritical to supercritical flows based on observed data. As a result, for the St. Charles River watershed, as shown in Fig. 12 (c), the subcritical flow requirement (i.e., frequency of subcritical conditions between 80%−100%) was met by 99.4% of the river reaches. For the À la Raquette River watershed, as shown in Fig. 12 (d), the subcritical flow regime is met by 100% of the reaches. As expected, the results of the *Fr* are directly related to the slope of the river reaches. This classification locates the reaches where the uncertainty of the HAND-SRC results is deemed acceptable; that is, the height-discharge relationship is theoretically unequivocal.

3.6. Flood event of April 2019

The study also evaluated the performance of the HAND-SRC model in generating first-instance flood maps using a flood event that occurred in April 2019 in southeastern Quebec. This flood was caused by a combination of snow melting and precipitation conditions, resulting in the highest recorded runoff volume in 57 years. Over a six-week period, from April 1st to May 15th, the area accumulated a total of 423 mm of precipitation, which was 113 mm more than the normal amount from 1981 to 2010 and 11 mm more than in 2017 (Quebec, 2019).

3.6.1. Performance metrics

The model's performance was evaluated by comparing the regulated risk zones identified by Quebec City, which considered flood levels of both 20 and 100 years, with the flood extent obtained by HAND-SRC. These flood-prone areas are the result of the development of rating curves in the watershed and have been incorporated into the city's development plan by the Quebec Water Expertise Direction, *Direction d'expertise hydrique du Québec* (DEH). Therefore, the comparison focused on the polygon corresponding to the floodplain zones (0–20 years) based on the available meteorological data to run a hydrological model.

The simulated discharge of April 27th 2019, was introduced into the SRC generated for each river segment in the St. Charles River sub-watershed. The discharge recorded at the gauge station on that day was 92.27 m^3/s, while HYDROTEL simulated 92.04 m^3/s. The drainage area and length of the main water course at this location are 119 km^2 and 21.9 km, respectively.

Fig. 13 depicts the depth and extent of the discharge introduced into each SRC based on the calibration at the gauge station. The hatched polygon corresponds to the regulated risk zones after the spring 2019 event. Furthermore, the water level in the simulated results is limited to the maximum value of the observed rating curve. Finally, the discontinuity observed in the figure is mainly due to the exclusion of river segments where the rating curve did not fit the observed curve (less than 3% of segments were excluded). A total of 29 SRCs were obtained at the St. Charles station by selecting those falling within ± 5% of PBIAS compared to the observed rating curve. From these, five random combinations of parameters were applied for all the river segments corresponding to the sub-

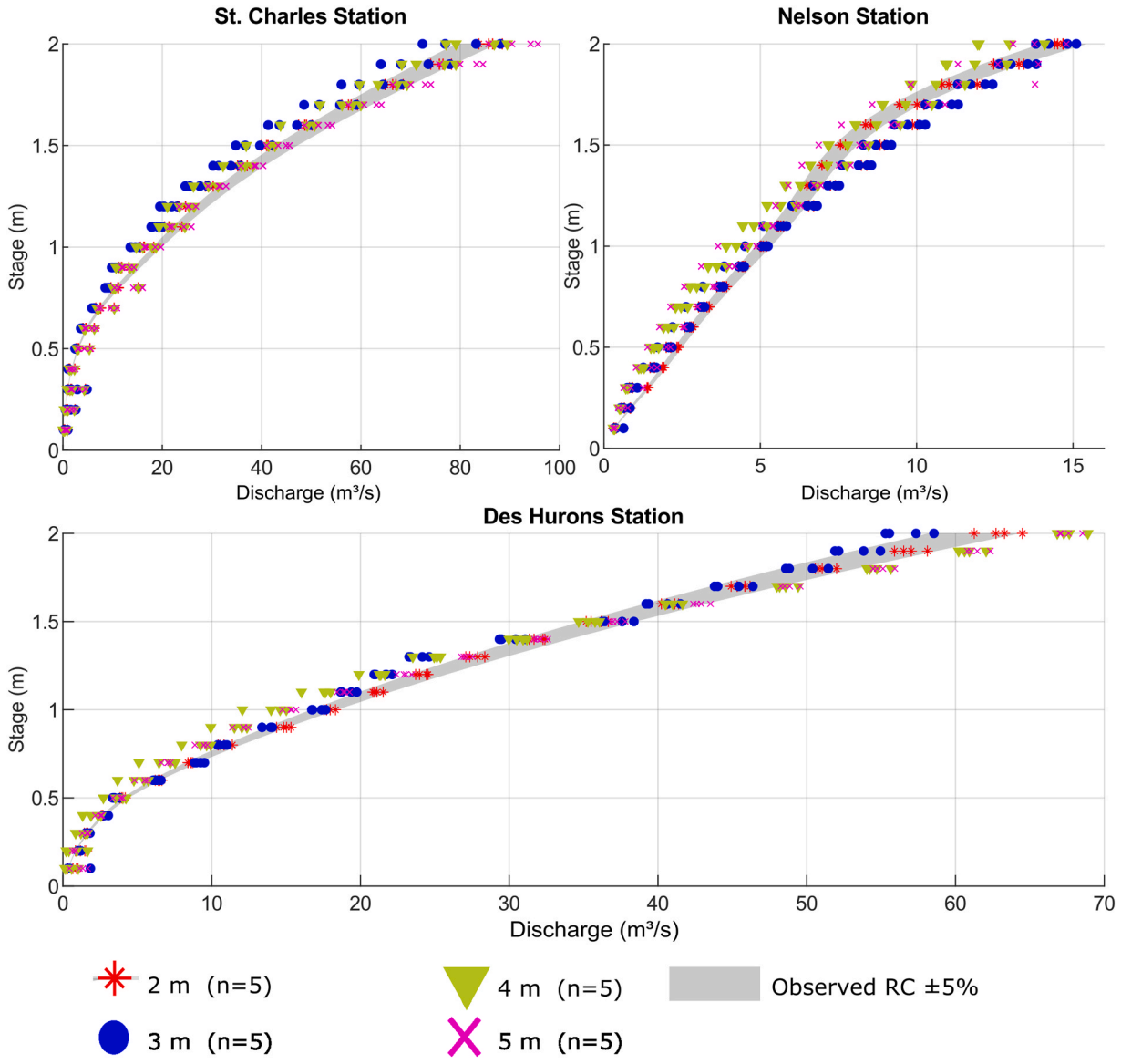

Fig. 9. Assessment of the spatial resolution effect for each gauge stations of the St. Charles River watershed. Four distinct resolutions (5 m, 4 m, 3 m, and 2 m) were tested based on the available data (DEM). While the 5 m resolution demonstrated satisfactory performance in terms of SRC, this analysis was crucial to highlight model's sensitivity to DEM resolution. The relationship between SRC and the representation of the river channel explain this sensitivity. However, it was also demonstrated that improving the resolution resulted in increased computation time.

watershed.

3.6.2. Binary flood map

The binary flood map when coupled with metrics such as overall accuracy, recall, F1 score, and the counts of true positives, false positives, false negatives, and true negatives, provides a comprehensive evaluation of a flood model's performance. The simulated flood was converted to a binary map to assess the calculation of the confusion matrix. Fig. 14 presents the results of the confusion matrix for the study area.

Table 6. introduces the quantitative performance of each parameter combination. The recall values for all combinations were above 70%, indicating the model's sensitivity to accurately detect True Positives. The precision values for all combinations were above 90%, indicating the model's ability to correctly identify positive values as true positives. These findings highlight the potential of integrating DEM and stream network data with HAND-SRC, along with the previously described rating curve selection method. This integration enables the production of floodplain maps for small watersheds where bathymetric data is unavailable.

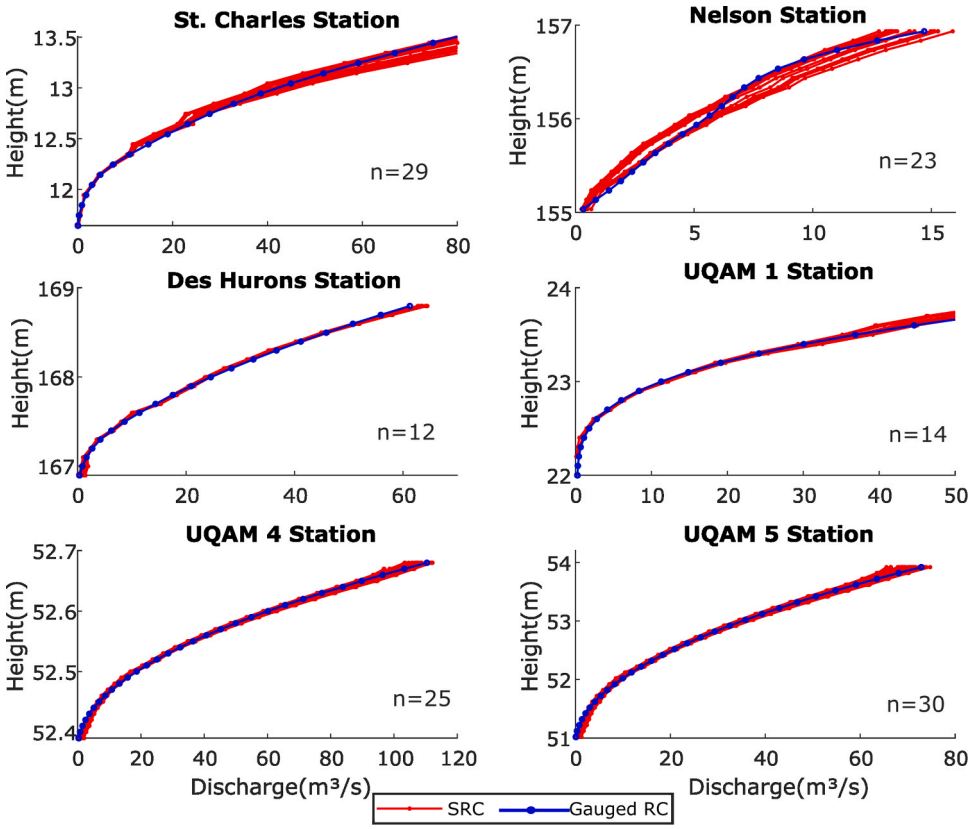

Fig. 10. Rating curves obtained after the Hit/Miss score. In the figure, the height corresponds to the elevation of each station above sea level.

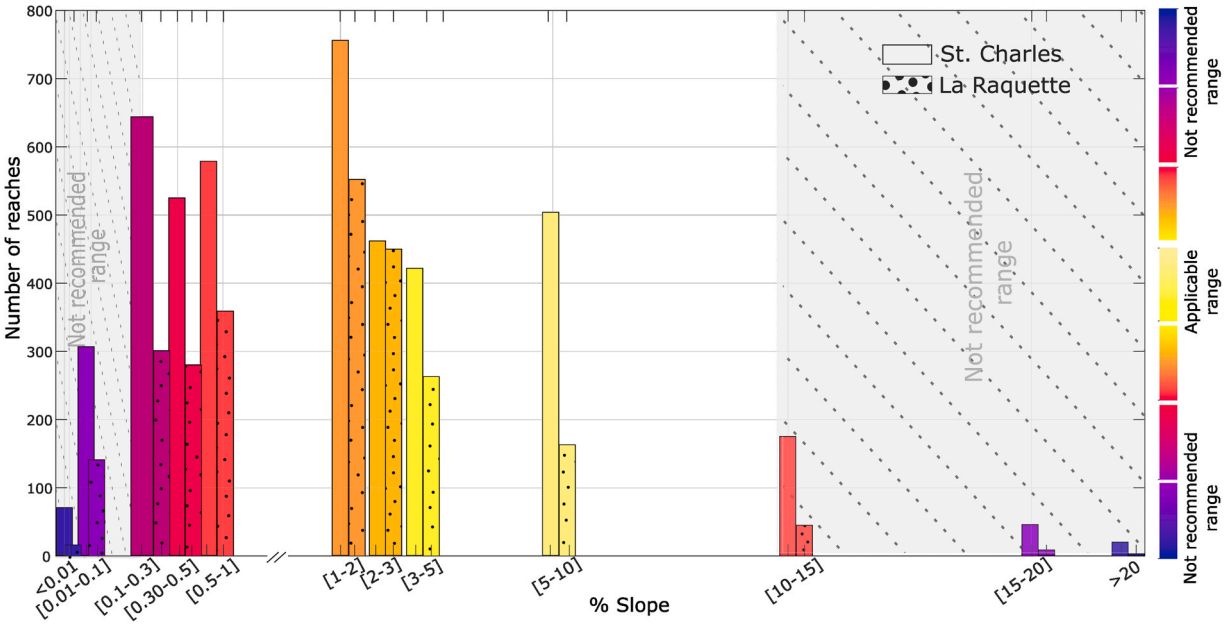

Fig. 11. Distribution of the river reach slopes for the À La Raquette River and St. Charles River watersheds.

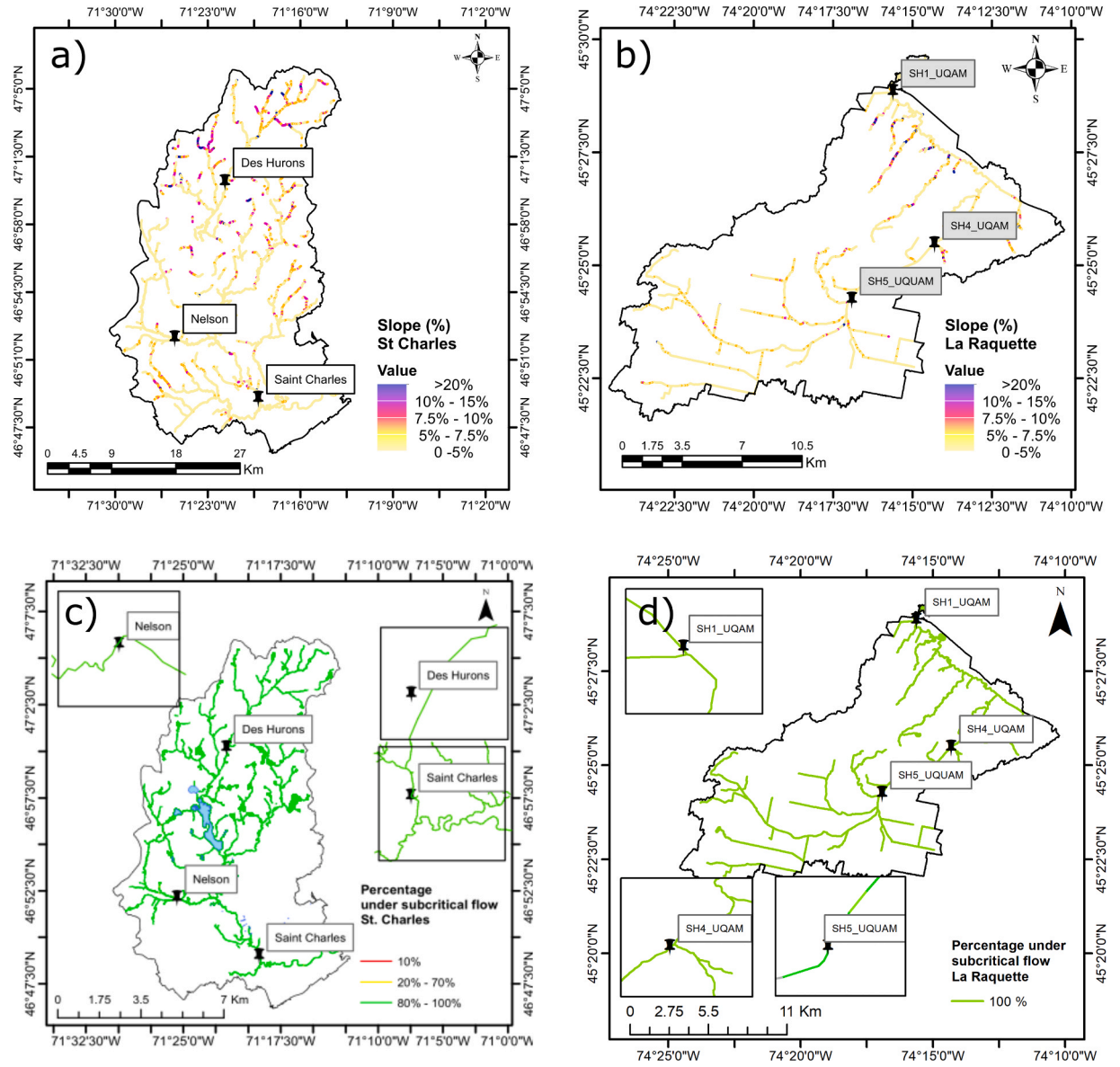

Fig. 12. Topomorphologic assessment for both watersheds. Classification of each river reach slope for the St. Charles River watershed (a), and À la Raquette River watershed (b). Classification of the HAND-SRC river reaches in terms of their frequency of flow reg regime unicity for the St. Charles River (c), and À la Raquette River watersheds (d).

4. Discussion

This study demonstrates the effectiveness of the HAND-SRC method in generating accurate synthetic rating curves (SRCs) and floodplain maps in small, ungauged watersheds, despite limitations in bathymetric data. Building on the work of Zheng et al. (2018), we refined the reach delineation, Manning coefficient selection, and calibration and validation approach to achieve accurate SRCs. Sensitivity analysis guided the calibration process by revealing parameter dynamics. Additionally, we used the Froude number and bed slope mapping to identify river reaches where the underlying assumptions could not be met. Simplified models like HAND are popular due to their ease of implementation, adaptable algorithms, and availability of gridded data. However, the HAND-SRC method has multiple uncertainties that need to be addressed, including key parameters like the Manning roughness coefficient, reach length, DEM resolution and uniform flow regimes for the Manning equation.

Regarding the Manning coefficient (n), Zheng et al. (2018) emphasized the use of land cover for determining "n" values. Although the authors did not explore the use of a compound value for n, they considered it a promising direction for enhancing the performance of the HAND-SRC method in the future. Furthermore, Scriven et al. (2021) found that combining a minimum and average value with a weighted n value improved SRC accuracy, especially in areas with medium to medium-high river gradients or river reaches under

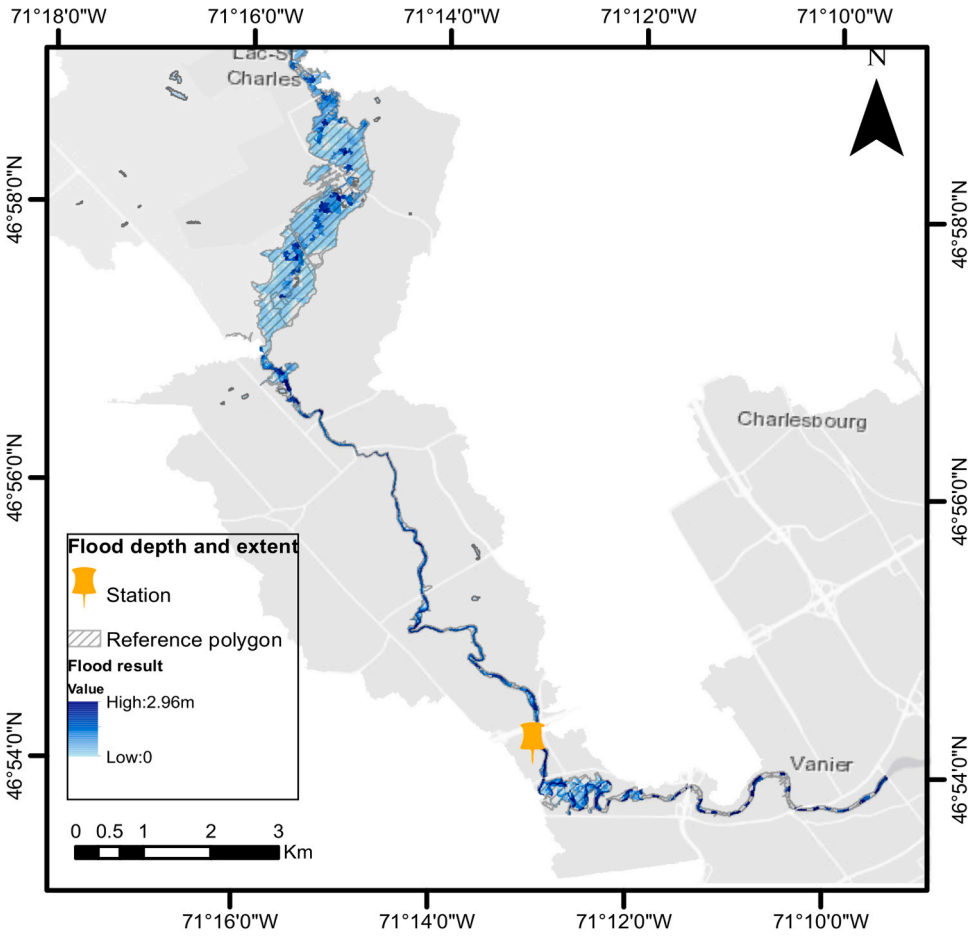

Fig. 13. Flood depth and extent of the St. Charles River sub watershed. The reference polygon corresponds to the delimitation provided by Quebec City based on the historical flood of spring 2019.

5 km. Additionally, Diehl et al. (2021) found that uncertainties in *n* contributed to approximately 20% and 40% of the variability in probabilistic HAND-based flood hazard maps. In this study, we employed a compound calculation of the roughness coefficient, based on the equation. Moreover, our sensitivity analysis not only revealed that reach length had a strong impact on the model's response but also confirmed the influence of different land cover coefficients, as shown in Fig. 6, aligning with previous research findings.

We also addressed the impact of vertical accuracy perturbations on SRC performance. Errors in elevation values can arise from noise or biases, affecting flow, slope, and connectivity. While higher resolution DEMs can reduce such uncertainties, statistical filtering methods are also effective noise removal. Indeed, DEM errors can affect the delineation of floodplain maps (Johnson et al., 2019). The decision to incorporate vertical resolution analysis resulted from the characteristics of the relatively narrow and short river reaches, which were found to be particularly sensitive to errors originating from the DEM, especially when compared to wider and longer reaches. Our analysis demonstrated and quantified the perturbations from Gaussian noise error in the DEM. As shown in Fig. 7, a vertical error increased the PBIAS from approximately 5% with the processed DEM to − 25.96% with the perturbed gridded data, highlighting the sensitivity of HAND-SRC to input DEM accuracy.

Furthermore, we assessed the influence of horizontal DEM resolution on the derivation of SRCs. Previous studies by Chaudhuri et al. (2021); Garousi-Nejad et al. (2019); Rebolho et al. (2018) have shown that higher DEM resolutions resulted in more accurate and detailed inundation maps. However, finer resolutions require more computation time and storage space. The authors of these studies suggested that the choice of DEM resolution should consider available data, objectives, and accuracy-cost trade-offs. In our study, we compared SRCs at different horizontal resolutions (5 m, 4 m, 3 m, 2 m) obtained by upscaling the original DEM. Our resolution approach did not compare the floodplain model; instead, it evaluated the accuracy of the SRCs in relation to the observed rating curves. However, once the SRCs were calibrated, we also addressed the comparison of floodplain model (see Section 3.2). Our findings presented Fig. 8, corroborated previous research results, confirming that finer resolutions improved SRC performance and reduced PBIAS from 11% to 5%. However, computation times increased by 40% for each rating curve calculation. Nevertheless, the HAND-SRC method remains competitive with high-resolution gridded data, as it allows for rapid rating curve calculations.

Comparisons to in-situ data also revealed uncertainties. Factors such as vegetation density and flow regimes introduce natural variability that affects stage-discharge relationships and the boundary conditions of hydraulic models (Le Coz et al., 2014; Rampinelli

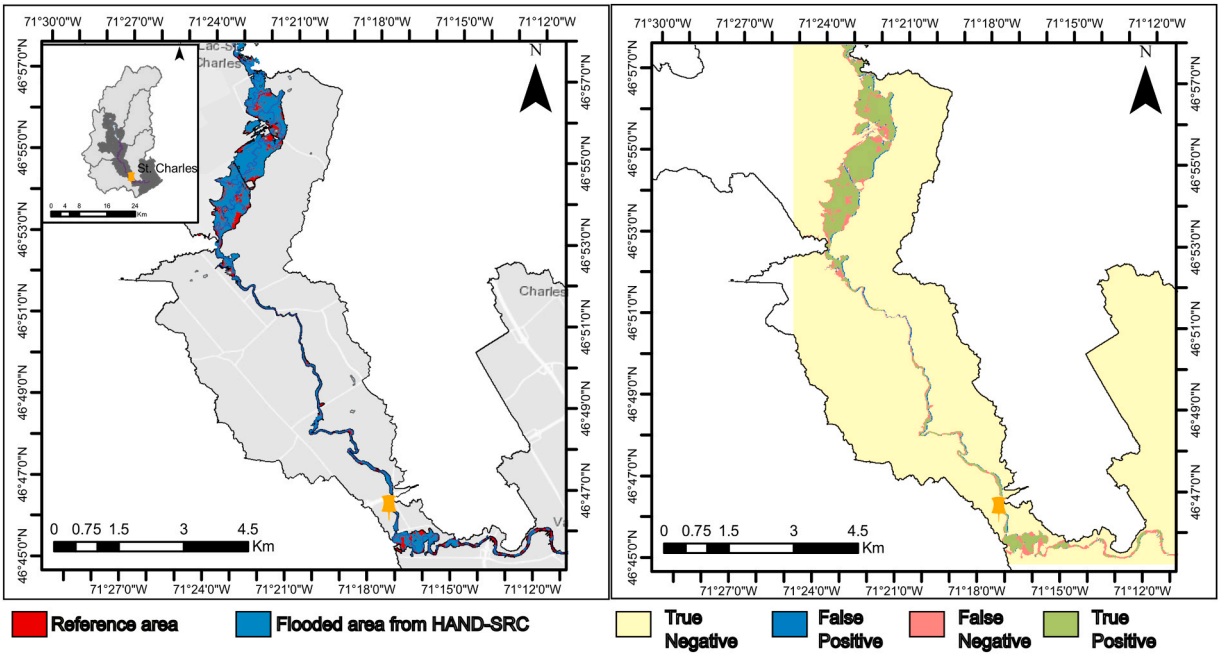

Fig. 14. Confusion matrix for the study area using randomly chosen parameters. (a). The result of the binary flood map derived from the model output. (b) This figure displays the distribution of the values calculated from the confusion matrix.

Table 6
Quantitative performances of different parameter combination after calibration at St. Charles gauge station. (OA) Overall accuracy, F1-score, Intersection over Union (IoU), Recall and Precision.

Combination	OA (%)	F1-Score (%)	IoU (%)	Recall (%)	Precision (%)
Comb-1	98.9	81.1	68.2	72.2	92.5
Comb-2	98.9	82.8	68.4	72.5	92.4
Comb-3	99.3	87.7	78.1	78.3	99.6
Comb-4	99.3	88.0	78.6	78.8	99.6
Comb-5	99.3	88.2	78.9	79.1	99.6

et al., 2020; Schmidt, 2004). Since inferring roughness coefficient values (*n)* from satellite images is challenging, we relied on values reported in Chow (1959). However, validating these selected values remains crucial in reducing uncertainty.

Given the absence of bathymetric data, our study proposed the use of the Froude number as a criterion to characterize potential flow regimes and ultimately validate the application of the Manning equation. The Froude number has also been used for developing of water depth and velocity maps, which are useful for comparing the performance of flood models developed from LiDAR images (Hauer et al. (2021) and identifying risk zones based on flow behavior (van Alphen et al., 2009). Other applications of the Froude number include determining the uncertainty associated with the stage-discharge curve (Schmidt, 2004) and comparing the performance between flood simulation models.

4.1. Application perspectives

Since this study does not use a probabilistic approach, applying an indicator based on the Froude number provides a measure of physical characteristics. In addition, this study is the first to include flow regime characteristics as a validation criterion for the HAND-SRC method. While there are uncertainties in applying the method in small watersheds, including more gauge stations can improve the results. This is because all upstream-derived SRCs (i.e., upstream of a gauge station) had a maximum discharge value equivalent to that of the nearest downstream gauge station. To compensate for the lack of gauge stations and accurately define each SRC's lower and upper discharge values, further work should explore the use of the drainage area of each river reach. Given the demonstrated impact of DEM resolution, we encourage the exploration of various strategies to mitigate this uncertainty, particularly for small river reaches that are susceptible to DEM errors. For further applications in Canada, data from the 2022 National Elevation Data Strategy update provides high-resolution LiDAR data covering more than 182,000 km^2 of the country (NRC, 2022). This dataset, in conjunction with hydrological information derived from remote sensing data, can be effectively employed with low-complexity models to support initial floodplain maps. This presents an opportunity to create preliminary floodplain maps that can subsequently be refined through more

complex analyses.

This study has demonstrated the potential of the HAND-SRC method to develop first-instance flood maps for small watersheds with limited hydrological data. The validation work, including the comparison with the 2019 flood in the St. Charles River watershed (Section 3.2.2), showed good performance in terms of overall accuracy (OA), precision, recall, F1 score and Intersection over Union (IoU). The results showed values of (OA) above 98%, recall values above 72%, F1 score above 88%, precision above 92%, and IoU above 68%. It should be noted that although the overall accuracy (OA) was calculated, it was not used to evaluate the model's performance due to its incorporated bias of this indicator. Indeed, it includes the TN (True Negative), which is in the overwhelming majority if the river does not flood substantially. The default parameter values presented in Section (3.1.2) achieved an OA of 97%, a recall rate of 47%, an F1 score of 64%, and an IoU of 32%. These results highlight the importance of calibration and its substantial impact on enhancing map accuracy. Similar studies have compared the accuracy of HAND for floodplain mapping using classification assessment. For instance, Aristizabal et al. (2020) reported recall values ranging between 30% and 85%. Furthermore, Li et al. (2022) conducted a similar assessment for two regions with an average size of 100 km ^{2}. They found that, for a 100-year flood event, recall values ranged between 73% and 80% and the overall accuracy between 93% and 94%. These results validate the performance demonstrated in our research. In terms of computation time, the rating curve calculation remained consistent between default and calibrated data. However, subsequent analyses such as GSA, calibration, and Froude number calculations require additional computational resources. Nevertheless, in this study, the latter stages of the HAND-SRC method have been automated and optimized to ensure efficient calculations. While the flood extent was compared, the sensitivity analysis provided guidance during the calibration process. It is important to note that the regulated risk zones and built-up areas for discharges were not evaluated for multiple events, as Scriven et al. (2021) did. However, their results also confirmed the potential of the HAND-SRC method for supporting floodplain mapping. Additionally, the comparison with the reference polygon can be subjective, as it can be produced differently by regional or local governments since flood information data is not centralized in Canada (Henstra et al., 2019). Nonetheless, our findings suggest that the HAND-SRC method can be valuable for developing flood maps in ungauged areas.

5. Conclusion

This paper introduced a novel methodology for obtaining and validating synthetic rating curves (SRC) in small watersheds, addressing a gap in the existing literature. While uncertainties remain regarding gridded data resolution and limited bathymetric data, the methodology provides a valuable first approximation for estimating hydraulic geometry and SRCs for small rivers.

Based on the proposed method, we derived SRCs with NRMSE values (in terms of observed discharges) between 0.03 and 0.62 and PBIAS values below $\pm$ 20% compared to gauged data across six stations. In addition, a Hit/Miss selection criteria identified at least ten calibrated curves per station with a PBIAS range of $\pm$ 5%. Meanwhile, global sensitivity analysis and assessing DEM resolution, Manning roughness coefficient, and reach length revealed the main sources of uncertainty to guide low-complexity model applications. Moreover, applying the Froude number as a validation criterion enabled the identification of applicable reaches, covering 100% and 99.4% of the À La Raquette River and St. Charles River watersheds, respectively. This supported, a first estimation of flood inundation in the studied small watersheds using low-complexity models despite lacking bathymetric data. Finally, the validation of a specific flood event in the St. Charles River watershed highlighted the potential of the method in small watersheds. Overall, this study demonstrated the potential of the HAND-SRC method for developing useful flood maps in ungauged areas and outlined promising research directions to expand applicability. The proposed methodology addresses a gap for small watersheds and provides a framework for first-approximation hydraulic geometry and floodplain delineation.

Funding

This research project was co-funded by a Mitacs Accelerate Program (project 554030) via the Quebec government 2013–2020 Action Plan on Climate Change, the watershed organization of the study region in partnership with Université Laval, Ville de Québec, Ouranos, OBV de la Capitale and the Natural Sciences and Engineering Research Council of Canada (NSERC) Discovery Grant program (grant to A.N. Rousseau).

CRediT authorship contribution statement

Camila A. Gordon: Investigation, data processing, and writing original draft. **Etienne Foulon:** supervision, methodology, writing and editing. **Alain N. Rousseau:** Methodology, supervision, revision, and editing.

Declaration of Competing Interest

The authors declare that they have no known competing financial interests or personal relationships that could have appeared to influence the work reported in this paper.

Data availability

Data will be made available on request.

Acknowledgement

The authors would like to acknowledge support from Marie-Larocque, professor at UQAM, and her research team for providing the rating curves for the three stations of the À la Raquette River watershed. We would like also to acknowledge *Ville de Québec*, for the precipitation data used to run HYDROTEL simulations.

References

Afshari, S., Tavakoly, A.A., Rajib, M.A., Zheng, X., Follum, M.L., Omranian, E., Fekete, B.M., 2018. Comparison of new generation low-complexity flood inundation mapping tools with a hydrodynamic model. J. Hydrol. 556, 539–556. https://doi.org/10.1016/j.jhydrol.2017.11.036.

van Alphen, J., Martini, F., Loat, R., Slomp, R., Passchier, R., 2009. Flood risk mapping in Europe, experiences and best practices. J. Flood Risk Manag. 2, 285–292. https://doi.org/10.1111/j.1753-318X.2009.01045.x.

Andreadis, K.M., Schumann, G.J.-P., Pavelsky, T., 2013. A simple global river bankfull width and depth database. Water Resour. Res. 49, 7164–7168. https://doi.org/10.1002/wrcr.20440.

Aristizabal, F., Judge, J., Monsivais-Huertero, A., 2020. High-resolution inundation mapping for heterogeneous land covers with synthetic aperture radar and terrain data. Remote Sens. 12 (6), 900.

Bates, P.D., De Roo, A.P.J., 2000. A simple raster-based model for flood inundation simulation. J. Hydrol. 236, 54–77. https://doi.org/10.1016/S0022-1694(00)00278-X.

Biancamaria, S., Andreadis, K.M., Durand, M., Clark, E.A., Rodriguez, E., Mognard, N.M., Alsdorf, D.E., Lettenmaier, D.P., Oudin, Y., 2010. Preliminary Characterization of SWOT Hydrology Error Budget and Global Capabilities. IEEE J. Sel. Top. Appl. Earth Obs. Remote Sens. 3, 6–19. https://doi.org/10.1109/JSTARS.2009.2034614.

Biancamaria, S., Lettenmaier, D.P., Pavelsky, T.M., 2016. The SWOT Mission and its capabilities for land hydrology. Surv. Geophys. 37 (2), 307–337. https://doi.org/10.1007/s10712-015-9346-y.

Bouda, M., Rousseau, A.N., Konan, B., Gagnon, P., Gumiere, S.J., 2012. Bayesian uncertainty analysis of the distributed hydrological model HYDROTEL. J. Hydrol. Eng. 17 (9), 1021–1032. https://doi.org/10.1061/(ASCE)HE.1943-5584.0000550.

Bouda, M., Rousseau, A.N., Gumiere, S.J., Gagnon, P., Konan, B., Moussa, R., 2014. Implementation of an automatic calibration procedure for HYDROTEL based on prior OAT sensitivity and complementary identifiability analysis. Hydrol. Process. 28 (12), 3947–3961. https://doi.org/10.1002/hyp.9882.

Chaudhuri, C., Gray, A., Robertson, C., 2021. InundatEd-v1.0: a height above nearest drainage (HAND)-based flood risk modeling system using a discrete global grid system. Geosci. Model Dev. 14 (6), 3295–3315. https://doi.org/10.5194/gmd-14-3295-2021.

Chow, V.T., 1959. Open-Channel Hydraulics. McGraw-Hill,, New York, NY.

Chow, V.T., Maidment, D.R., Mays, L.W., 1988. Applied Hydrology, Vol. 149. McGraw-Hill Company,, New York, NY.

Crosato, A., Zulfan, J., Vargas-Luna, A., 2020. Improved floodplain vegetation roughness for 1D hydraulic models. *2020*. In: In *River Flow*, Vol. 1. CRC Press,, pp. 1139–1147. https://doi.org/10.1201/b22619-159. *2020*.

Diehl, R.M., Gourevitch, J.D., Drago, S., Wemple, B.C., 2021. Improving flood hazard datasets using a low-complexity, probabilistic floodplain mapping approach. Plos One 16 (3), e0248683. https://doi.org/10.1371/journal.pone.0248683.

ECCC. (2020). Canada's Top 10 Weather Stories of 2019. Environment and Climate Change Canada Government of Canada. Retrieved 25/11 from https://www.canada.ca/en/environment-climate-change/services/top-ten-weather-stories/2019.html.

Einstein, H., 1934. Der hydraulische oder profil-radius. Schweiz. Bauztg. 103 (8), 89–91.

Fernandes, J.N., 2021. Apparent roughness coefficient in overbank flows. SN Appl. Sci. 3 (7), 696.

Fortin, J.-P., Turcotte, R., Massicotte, S., Moussa, R., Fitzback, J., Villeneuve, J.-P., 2001. Distributed watershed model compatible with remote sensing and GIS data. I: Description of model. J. Hydrol. Eng. 6 (2), 91–99. https://doi.org/10.1061/(ASCE)1084-0699(2001)6:2(100)).

Garousi-Nejad, I., Tarboton, D.G., Aboutalebi, M., Torres-Rua, A.F., 2019. Terrain Analysis Enhancements to the Height Above Nearest Drainage Flood Inundation Mapping Method. Water Resour. Res. 55, 7983–8009. https://doi.org/10.1029/2019WR024837.

Ghanghas, A., Dey, S., Merwade, V., 2022. Evaluating the reliability of synthetic rating curves for continental scale flood mapping. J. Hydrol. 606, 127470 https://doi.org/10.1016/j.jhydrol.2022.127470.

Godbout, L., Zheng, J.Y., Dey, S., Eyelade, D., Maidment, D., Passalacqua, P., 2019. Error Assessment for Height Above the Nearest Drainage Inundation Mapping. JAWRA J. Am. Water Resour. Assoc. 55, 952–963. https://doi.org/10.1111/1752-1688.12783.

Gomes Jr, M.N., Rápalo, L.M., Oliveira, P.T., Giacomoni, M.H., do Lago, C.A., Mendiondo, E.M., 2023. Modeling unsteady and steady 1D hydrodynamics under different hydraulic conceptualizations: Model/Software development and case studies. Environ. Model. Softw., 105733

Hauer, C., Flödl, P., Habersack, H., Pulg, U., 2021. Critical flows in semi-alluvial channels during extraordinarily high discharges: Implications for flood risk management. J. Flood Risk Manag. 14 (4), e12741 https://doi.org/10.1111/jfr3.12741.

Henderson, F.M. (1966). *Open Channel Flow* Macmillan. New York, NY.

Hengl, T., 2006. Finding the right pixel size. Comput. Geosci. 32 (9), 1283–1298. https://doi.org/10.1016/j.cageo.2005.11.008.

Henstra, D., Minano, A., Thistlethwaite, J., 2019. Communicating disaster risk? An evaluation of the availability and quality of flood maps. Nat. Hazards Earth Syst. Sci. 19 (1), 313–323. https://doi.org/10.5194/nhess-19-313-2019.

Heuvelink, G.B., 1998. London. Error propagation in environmental modelling with GIS. CRC press,. https://doi.org/10.4324/9780203016114.

Hirabayashi, Y., Mahendran, R., Koirala, S., Konoshima, L., Yamazaki, D., Watanabe, S., Kim, H., Kanae, S., 2013. Global flood risk under climate change. Nat. Clim. Change 3, 816–821. https://doi.org/10.1038/nclimate1911.

Horton, R.E., 1933. Separate roughness coefficients for channel bottom and sides. Eng. N. -Rec. 111 (22), 652–653.

IBC. (2020). Investing in Canada's future: The cost of Climate adaptation at the local level.

Jafarzadegan, K., Merwade, V., Saksena, S., 2018. A geomorphic approach to 100-year floodplain mapping for the Conterminous United States. J. Hydrol. 561, 43–58. https://doi.org/10.1016/j.jhydrol.2018.03.061.

Johnson, J.M., Munasinghe, D., Eyelade, D., Cohen, S., 2019. An integrated evaluation of the National Water Model (NWM)–Height Above Nearest Drainage (HAND) flood mapping methodology. Nat. Hazards Earth Syst. Sci. 19 (11), 2405–2420. https://doi.org/10.5194/nhess-19-2405-2019.

Jonkman, S.N., 2005. Global Perspectives on Loss of Human Life Caused by Floods. Nat. Hazards 34, 151–175. https://doi.org/10.1007/s11069-004-8891-3.

Kim, M.H., Morlock, S.E., Arihood, L.D., & Kiesler, J.L. (2011). Observed and Forecast Flood-Inundation Mapping Application: A Pilot Study of an Eleven-Mile Reach of the White River, Indianapolis, Indiana.

Le Coz, J., Renard, B., Bonnifait, L., Branger, F., Le Boursicaud, R., 2014. Combining hydraulic knowledge and uncertain gaugings in the estimation of hydrometric rating curves: A Bayesian approach. J. Hydrol. 509, 573–587. https://doi.org/10.1016/j.jhydrol.2013.11.016.

Leopold, L.B., & Maddock, T.J. (1953). *The Hydraulic Geometry of Stream Channels and Some Physiographic Implications* (Professional Paper, Issue. U. S. G. P. Office.

Li, Z., Mount, J., Demir, I., 2022. Accounting for uncertainty in real-time flood inundation mapping using HAND model: Iowa case study. Nat. Hazards 112 (1), 977–1004. https://doi.org/10.1007/s11069-022-05215-z.

Maidment, D.R., 1992. Handbook of hydrology. McGraw Hill, Inc,, Austin,TX.

Mays, L.W., 2005. Water Resources Engineering. John Wiley & Sons,, Hoboken, NJ.

McGrath, H., Bourgon, J.-F., Proulx-Bourque, J.-S., Nastev, M., Abo El Ezz, A., 2018. A comparison of simplified conceptual models for rapid web-based flood inundation mapping. Nat. Hazards 93 (2), 905–920. https://doi.org/10.1007/s11069-018-3331-y.

MELCC. (2019). *Utilisation du territoire 2019*. Ministère de l'Environnement et de la Lutte contre les changements climatiques (MELCC). https://www.donneesquebec.ca/recherche/fr/dataset/utilisation-du-territoire.
MERN. (2021). COUCHE DES POINTS GÉODÉSIQUES (Structure physique des données, Issue. https://diffusion.mern.gouv.qc.ca/diffusion/RGQ/Documentation/Geodesie/StructurePhysique_PointsGeodesiques.pdf.
MERN. (2022). Géobase du réseau hydrographique du Québec (GRHQ). Ministère de l'Énergie et des Ressources naturelles. https://mern.gouv.qc.ca/repertoire-geographique/reseau-hydrographique-grhq/.
MFFP. (2020). LiDAR - Modèles numériques (terrain, canopée, pente) LiDAR - Modèles numériques (terrain, canopée, pente).
Morris, M.D., 1991. Factorial sampling plans for preliminary computational experiments. Technometrics 33 (2), 161–174.
Musser, J.W., & Dyar, T.R. (2007). *Two-dimensional floodinundation model of the Flint River* (Vol. 5107). US Geological Survey. Albany, GA.
Nobre, A.D., Cuartas, L.A., Hodnett, M., Rennó, C.D., Rodrigues, G., Silveira, A., Waterloo, M., Saleska, S., 2011. Height Above the Nearest Drainage - a hydrologically relevant new terrain model. J. Hydrol. 404, 13–29. https://doi.org/10.1016/j.jhydrol.2011.03.051.
Noël, P., Rousseau, A.N., Paniconi, C., Nadeau, D.F., 2014. Algorithm for Delineating and Extracting Hillslopes and Hillslope Width Functions from Gridded Elevation Data. J. Hydrol. Eng. 19, 8865–8901. https://doi.org/10.1061/(asce)he.1943-5584.0000783.
NRC. (2022). National Elevation Data Strategy update fall 2022. N. R. Canada. https://ftp.maps.canada.ca/pub/nrcan_rncan/publications/STPublications_PublicationsST/331/331359/gid_331359.pdf.
Pelletier, P.M., 1988. Uncertainties in the single determination of river discharge: a literature review. Can. J. Civ. Eng. 15 (5), 834–850. https://doi.org/10.1139/l88-109.
Pianosi, F., Wagener, T., 2016. Understanding the time-varying importance of different uncertainty sources in hydrological modelling using global sensitivity analysis. Hydrol. Process. 30, 3991–4003. https://doi.org/10.1002/hyp.10968.
Pianosi, F., Sarrazin, F., Wagener, T., 2015. A Matlab toolbox for Global Sensitivity Analysis. Environ. Model. Softw. 70, 80–85. https://doi.org/10.1016/j.envsoft.2015.04.009.
Polidori, L., El Hage, M., 2020. Digital Elevation Model Quality Assessment Methods: A Critical Review. Remote Sens. 12 (21), 3522. https://doi.org/10.3390/rs12213522.
Quebec, V. d. (2019). RÉVISION DES COTES DE CRUES Rivière Saint-Charles – Tronçon 5 Amont du seuil du secteur du Château-d'Eau à l'aval du barrage Cyrille-Delage. https://www.ville.quebec.qc.ca/citoyens/propriete/docs/zones_inondables/saint_charles_troncon5/rapport_cotes_crues_saintcharles_VQ20140620_troncon5.pdf.
Quintero, F., Rojas, M., Muste, M., Krajewski, W.F., Perez, G., Johnson, S., Anderson, A., Hunemuller, T., Cappuccio, B., Zogg, J., 2021. Development of Synthetic Rating Curves: Case Study in Iowa. J. Hydrol. Eng. 26 (1), 05020046 https://doi.org/10.1061/(ASCE)HE.1943-5584.0002022.
Rampinelli, C.G., Knack, I., Smith, T., 2020. Flood Mapping Uncertainty from a Restoration Perspective: A Practical Case Study. Water 12, 1948. https://doi.org/10.3390/w12071948.
Rantz, S.E. (1982). *Measurement and computation of streamflow: Measurement of stage and discharge.* (Geological Survey Water-Supply Paper 2175, Issue.
Razavi, S., Gupta, H.V., 2016a. A new framework for comprehensive, robust, and efficient global sensitivity analysis: 1. Theory. Water Resour. Res. 52 (1), 423–439. https://doi.org/10.1002/2015WR017558.
Razavi, S., Gupta, H.V., 2016b. A new framework for comprehensive, robust, and efficient global sensitivity analysis: 2. Application. Water Resour. Res. 52 (1), 440–455. https://doi.org/10.1002/2015WR017559.
Rebolho, C., Andréassian, V., Le Moine, N., 2018. Inundation mapping based on reach-scale effective geometry. Hydrol. Earth Syst. Sci. 22, 5967–5985. https://doi.org/10.5194/hess-22-5967-2018.
Rennó, C.D., Nobre, A.D., Cuartas, L.A., Soares, J.V., Hodnett, M.G., Tomasella, J., Waterloo, M.J., 2008. HAND, a new terrain descriptor using SRTM-DEM: Mapping terra-firme rainforest environments in Amazonia. Remote Sens. Environ. 112 (9), 3469–3481. https://doi.org/10.1016/j.rse.2008.03.018.
Rousseau, A.N., Fortin, J.-P., Turcotte, R., Royer, A., Savary, S., Quévy, F., Noël, P., Paniconi, C., 2011. PHYSITEL, a specialized GIS for supporting the implementation of distributed hydrological models. Water N. 18–20.
Samela, C., Troy, T.J., Manfreda, S., 2017. Geomorphic classifiers for flood-prone areas delineation for data-scarce environments. Adv. Water Resour. 102, 13–28. https://doi.org/10.1016/j.advwatres.2017.01.007.
Sangwan, N., Merwade, V., 2015. A Faster and Economical Approach to Floodplain Mapping Using Soil Information. JAWRA J. Am. Water Resour. Assoc. 51 (5), 1286–1304. https://doi.org/10.1111/1752-1688.12306.
Savage, J.T.S., Pianosi, F., Bates, P., Freer, J., Wagener, T., 2016. Quantifying the importance of spatial resolution and other factors through global sensitivity analysis of a flood inundation model. Water Resour. Res. 52 (11), 9146–9163. https://doi.org/10.1002/2015WR018198.
Schmidt, A.R. (2004). Application of Point-Estimation Method to Calculate Uncertainties in Discharges from Stage-Discharge Ratings. Critical Transitions in Water and Environmental Resources Management, Reston, VA.
Scriven, B.W.G., McGrath, H., Stefanakis, E., 2021. GIS derived synthetic rating curves and HAND model to support on-the-fly flood mapping. Nat. Hazards 109 (2), 1629–1653. https://doi.org/10.1007/s11069-021-04892-6.
Sobol′, I.M., 2001. Global sensitivity indices for nonlinear mathematical models and their Monte Carlo estimates. Math. Comput. Simul. 55, 271–280. https://doi.org/10.1016/S0378-4754(00)00270-6.
Tayefi, V., Lane, S.N., Hardy, R.J., Yu, D., 2007. A comparison of one- and two-dimensional approaches to modelling flood inundation over complex upland floodplains. Hydrol. Process. 21, 3190–3202. https://doi.org/10.1002/hyp.6523.
Teng, J., Jakeman, A.J., Vaze, J., Croke, B.F.W., Dutta, D., Kim, S., 2017. Flood inundation modelling: A review of methods, recent advances and uncertainty analysis. Environ. Model. Softw. 90, 201–2016. https://doi.org/10.1016/j.envsoft.2017.01.006.
Turcotte, B., Burrell, B.C., & Beltaos, S. (2019). The Impact of Climate Change on Breakup Ice Jams in Canada: State of knowledge and research approaches. 20th Workshop on the Hydraulics of Ice Covered Rivers, Ottawa,ON.
Turcotte, R., Rousseau, A.N., Fortin, J.-P., Villeneuve, J.-P., 2003. A Process-Oriented, Multiple-Objective Calibration Strategy Accounting for Model Structure. *Calibration Watershed Models* 153–163. https://doi.org/10.1002/9781118665671.ch11.
Turcotte, R., Fortin, L.-G., Fortin, V., Fortin, J.-P., Villeneuve, J.-P., 2007. Operational analysis of the spatial distribution and the temporal evolution of the snowpack water equivalent in southern Québec, Canada. Hydrol. Res. 38 (3), 211–234. https://doi.org/10.2166/nh.2007.009.
Yahaya, S. (2008). *Multicriteria analysis for flood vulnerable areas in hadejia-jama'are river Basin*, Nigeria American Society for Photogrammetry and Remote Sensing - ASPRS Annual Conference 2008 - Bridging the Horizons: New Frontiers in Geospatial Collaboration,
Yapo, P.O., Gupta, H.V., Sorooshian, S., 1996. Automatic calibration of conceptual rainfall-runoff models: sensitivity to calibration data. J. Hydrol. 181, 23–48. https://doi.org/10.1016/0022-1694(95)02918-4.
Zheng, X., Tarboton, D.G., Maidment, D.R., Liu, Y.Y., Passalacqua, P., 2018. River Channel Geometry and Rating Curve Estimation Using Height above the Nearest Drainage. J. Am. Water Resour. Assoc. 54, 785–806. https://doi.org/10.1111/1752-1688.12661.
Zokagoa, J.M., Soulaïmani, A., Dupuis, P., 2021. Flood risk mapping using uncertainty propagation analysis on a peak discharge: case study of the Mille Iles River in Quebec. Nat. Hazards 107, 285–310. https://doi.org/10.1007/s11069-021-04583-2.